MECHANISM AND KINETICS OF FISCHER-TROPSCH SYNTHESIS OVER SUPPORTED RUTHENIUM CATALYSTS

CALIFORNIA UNIV., LIVERMORE. LAWRENCE
LIVERMORE LAB

JUN 1981

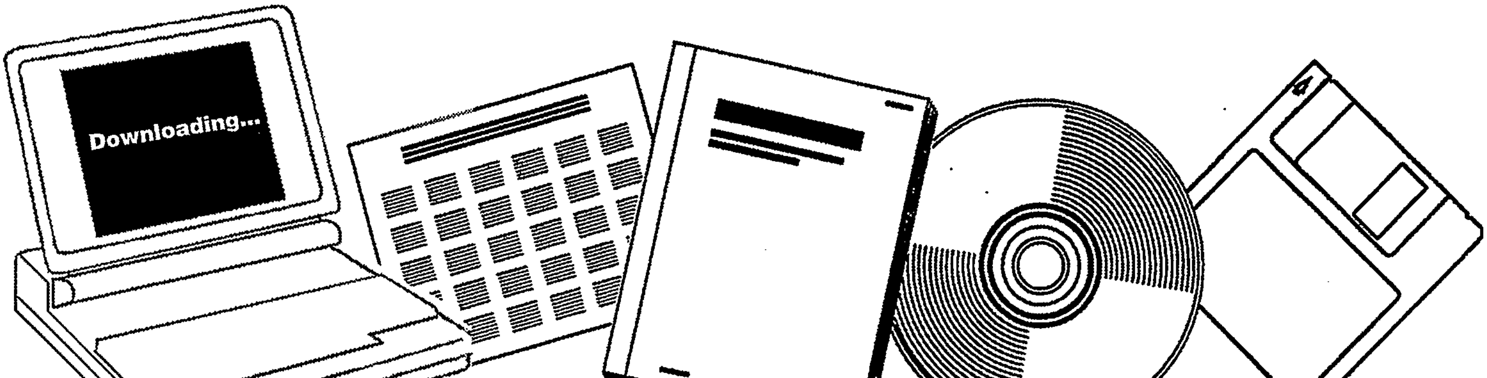

One Source. One Search. One Solution.

NTIS

Providing Permanent, Easy Access to U.S. Government Information

National Technical Information Service is the nation's largest repository and disseminator of government-initiated scientific, technical, engineering, and related business information. The NTIS collection includes almost 3,000,000 information products in a variety of formats: electronic download, online access, CD-ROM, magnetic tape, diskette, multimedia, microfiche and paper.

Search the NTIS Database from 1990 forward
NTIS has upgraded its bibliographic database system and has made all entries since 1990 searchable on **www.ntis.gov.** You now have access to information on more than 600,000 government research information products from this web site.

Link to Full Text Documents at Government Web Sites
Because many Government agencies have their most recent reports available on their own web site, we have added links directly to these reports. When available, you will see a link on the right side of the bibliographic screen.

Download Publications (1997 - Present)
NTIS can now provides the full text of reports as downloadable PDF files. This means that when an agency stops maintaining a report on the web, NTIS will offer a downloadable version. There is a nominal fee for each download for most publications.

For more information visit our website:

www.ntis.gov

U.S. DEPARTMENT OF COMMERCE
Technology Administration
National Technical Information Service
Springfield, VA 22161

Lawrence Berkeley Laboratory
UNIVERSITY OF CALIFORNIA

Materials & Molecular
Research Division

THE MECHANISM AND KINETICS OF FISCHER-TROPSCH SYNTHESIS OVER SUPPORTED RUTHENIUM CATALYSTS

Carl Stephen Kellner
(Ph.D. thesis)

June 1981

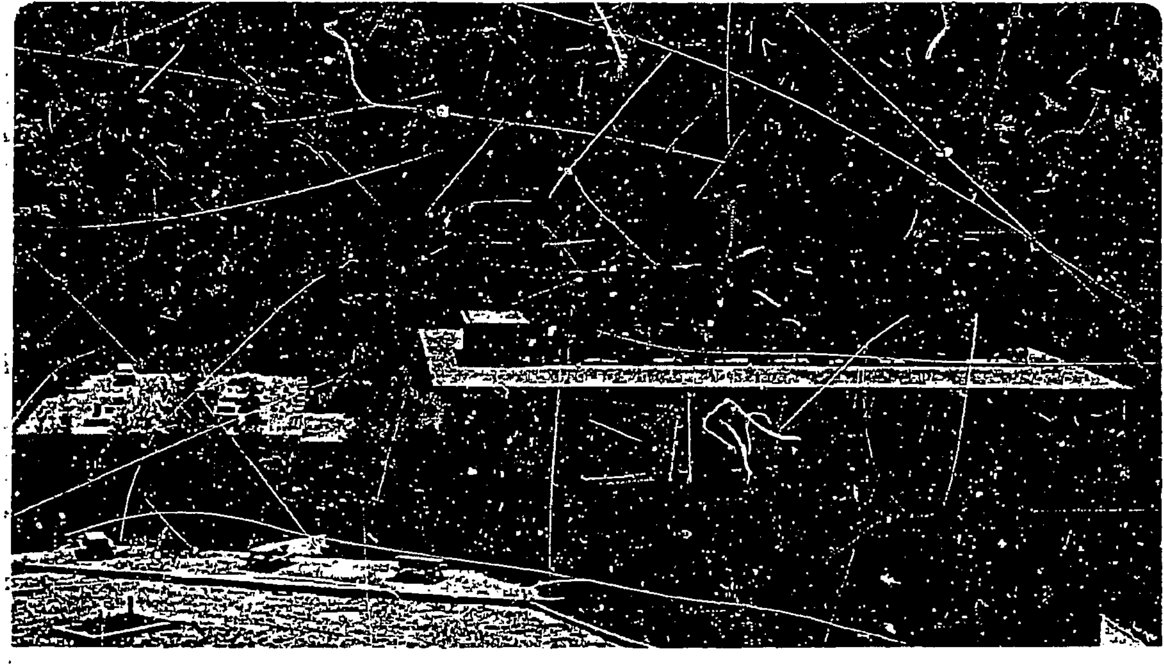

Prepared for the U.S. Department of Energy under Contract W-7405-ENG-48

LBL-12278

THE MECHANISM AND KINETICS OF FISCHER-TROPSCH SYNTHESIS OVER SUPPORTED RUTHENIUM CATALYSTS

Carl Stephen Kellner

Materials and Molecular Research Division
Lawrence Berkeley Laboratory and Department of Chemical Engineering
University of California, Berkeley, California 94720

Ph.D. Thesis

June 1981

This work was supported by the Director, Office of Energy Research, Office of Basic Energy Sciences, Chemical Sciences Division of the U. S. Department of Energy under Contract No. W-7405-ENG-48.

TABLE OF CONTENTS

LIST OF TABLES

Chapter II

Chapter IV

Chapter V

Chapter VI

LIST OF FIGURES

Chapter II

Chapter III

Appendix I

Appendix II

The Mechanism and Kinetics of Fischer-Tropsch Synthesis Over Supported Ruthenium Catalysts

Carl Stephen Kellner

Materials and Molecular Research Division
Lawrence Berkeley Laboratory

and

Department of Chemical Engineering
University of California, Berkeley, CA 94720

ABSTRACT

A detailed study of the kinetics of the Fischer-Tropsch synthesis of hydrocarbons, methanol, and acetaldehyde, over alumina- and silica-supported ruthenium catalysts has been carried out over a broad range of reaction conditions. Based on these results and information taken from the literature, mechanisms for the formation of normal paraffins, α-olefins, methanol, and acetaldehyde have been proposed.

Rate data were obtained between 448 and 548K, 1 and 10 atm, and H_2/CO ratios between 1 and 3, utilizing a micro flow reactor operated at very low conversions. These conditions allowed the intrinsic reaction kinetics to be observed with minimal interference from secondary reactions. In addition to the studies performed with H_2/CO mixtures, a series of experiments were carried out utilizing D_2/CO mixtures. These studies were used to help identify rate limited steps and steps that were at equilibrium.

A complementary investigation, carried out by *in situ* infrared spectroscopy, was performed using a Fourier Transform spectrometer. The spectra obtained were used to identify the modes of CO adsorption,

the CO coverage, and the relative reactivity of different forms of adsorbed CO. It was established that CO adsorbs on alumina-supported Ru in, at least, two forms: i)Ru-CO and ii)OC-Ru-CO. Only the first of these forms participates in CO hydrogenation. The coverage of this species is described by a simple Langmuir isotherm.

The kinetics of hydrocarbon synthesis, the olefin to paraffin ratio for each product, and the probability of chain propagation can all be interpreted on the basis of the reaction mechanism described below. Reaction is initiated by the adsorption of CO and its subsequent dissociation. Atomic oxygen is rejected as H_2O and the carbon undergoes stepwise hydrogenation to form $CH_x (x=1-3)$ species. Methane is formed by reductive elimination of methyl groups while the formation of higher molecular weight products is initiated by the addition of a CH_2 unit to an adsorbed CH_3 group. Further chain growth then proceeds via a similar process. Olefins are formed by β-elimination of hydrogen from an adsorbed alkyl group and paraffins are formed by reductive elimination of an alkyl group. Rate expressions based on this mechanism are reasonably consistent with the experimental data.

Acetaldehyde, obtained mainly over silica-supported Ru, appears to be formed by a mechanism related to that for hydroformulation of olefins. Following the formation of methyl groups, as discussed above, CO is inserted into the metal-carbon bond of the CH_3 group. The resulting acetyl species then undergoes reductive elimination to produce acetaldehyde. Methanol, rather than acetaldehyde, is observed over alumina-supported Ru. The mechanism by which this product is formed is not clear. However, the observed kinetics are consistent with a mechanism in which μ-bridge adsorbed CO is hydrogenated to form a methoxy intermediate. Reductive elimination of this moiety results in methanol formation.

The effect of the dispersion of Ru/Al_2O_3 catalysts on their specific activity and selectivity was also investigated. The specific activity for all products decreased rapidly with increasing dispersion; a particularly rapid fall off being observed for dispersions greater than 0.7. The olefin to paraffin ratio of the products and the probability of chain growth were nearly independent of dispersion for dispersions less than 0.6 but decreased sharply at higher dispersions. The origin of the dispersion effects are not fully understood. It may be hypothesized that at least a part of the observed effects is due to changes in the electronic properties of the small Ru particles constituting the catalyst.

CHAPTER I

INTRODUCTION

The Fischer-Tropsch synthesis, a catalytic process by which hydrocarbons and oxygen-containing products are produced from carbon monoxide and hydrogen, has attracted a great deal of attention in the last decade. This interest stems largely from the potential of utilizing Fischer-Tropsch synthesis (FTS) to produce transportation fuels and chemical feedstocks from coal. While a very large amount of empirical data (1) have been obtained on catalyst and process performance since the 1920's, when FTS was developed into a viable process (2), only recently have some of the fundamental reactions occurring on the catalyst surface begun to be understood (3,4). Much of what is known about the mechanism of FTS has been obtained through studies of related, homogeneously catalysed, reactions (5,6) but more detailed studies, performed with supported, heterogeneous, catalysts, are still required to develop a clearer understanding of the overall surface chemistry. Development of such information is highly desirable since it could aid in guiding the synthesis of selected products or ranges of products.

Although many of the transition metals will catalyse the reaction between CO and H_2, iron, cobalt, and ruthenium are the most selective for the synthesis of intermediate molecular weight hydrocarbons(1). Of the three, ruthenium has a number of properties that make it particularly attractive as a model catalyst for a fundamental study of FTS. It possesses both high intrinsic activity and selectivity for straight chain product formation and produces few oxygen containing products. It can be reduced readily in flowing hydrogen, is easily supported in highly dispersed form, and because ruthenium does not form a bulk carbide or oxide under Fischer-Tropsch reaction conditions, as do iron and cobalt, a long induction period is not required prior to the onset of FTS. These properties of ruthenium facilitate the acquisition and interpretation of kinetic data.

The objectives of the present study are to reexamine the kinetics of FTS over supported Ru catalysts, to determine whether these results are compatible with the current understanding of the mechanisms of FTS, and, when possible, to discriminate between plausible, parallel, reaction pathways. To this end, the kinetics of C_1 through C_{10} paraffin and olefin formation have been determined, over Ru/Al_2O_3 and Ru/SiO_2 catalysts, over a broad range of realistic Fischer-Tropsch reaction conditions. The pressure has been varied from 1 to 10 atm, the temperature from 448 to 548K, and the H_2/CO ratio from 1 to 3. However, rather than operating at the high conversions typical of an industrial process, conversions have been kept below 2% in order that the intrinsic kinetics could be observed. The kinetics of methanol and acetaldehyde formation, the most abundant organic oxygen containing products observed over Ru/Al_2O_3 and Ru/SiO_2 catalysts, respectively, have also been investigated.

Because kinetic data alone is rarely capable of discriminating between similar reaction mechanisms (4), additional information has been obtained by in situ infrared spectroscopy of the catalyst during reaction and by carrying out a series of runs using D_2/CO rather than H_2/CO mixtures. In situ infrared spectroscopic studies allow the types of adsorbed species present on the catalyst surface to be determined

(7) and, in addition, provides a method by which changes in the concentrations of these species with reaction conditions or time can be observed. Various types of experiments can be carried out with isotopically labeled reactants (8). In the present study the focus has been on determining how using D_2/CO in the place of H_2/CO mixtures effects the observed reaction rates. From such information, conclusions can be drawn concerning the nature of elementary steps involving the transfer of hydrogen atoms.

The influence of Ru dispersion on catalyst activity and selectivity has also been investigated as part of this effort. Previous studies have demonstrated that metal dispersion can have an effect on catalyst activity and selectivity (9). The purpose of these studies is to establish the extent to which dispersions can be used to alter the distribution of products obtained.

The balance of this thesis is divided into five parts, reflecting individual efforts undertaken in the course of this work. A review of the literature pertaining to each effort is presented at the beginning of each chapter. Chapter II deals with the interpretation of H_2/D_2 isotope effects observed during the synthesis of methane and higher molecular weight hydrocarbons. The results of in situ infrared studies are discussed in Chapter III. Determination of the kinetics of hydrocarbon synthesis is discussed in Chapter IV and the experimental data are compared with rate and product distribution expressions derived on the basis of a proposed mechanism. In Chapter V observations of methanol and acetaldehyde synthesis are discussed in the light of mechanisms for the formation of these products. Finally, Chapter VI deals with the effect of the dispersion of Ru/Al_2O_3 on the activity and selectivity of these catalysts. Several appendices dealing with experimental apparatus and procedures appear at the end of the thesis.

REFERENCES

1. Storch, H., Golumbic, N., and Anderson, R., "The Fischer-Tropsch and Related Synthesis", Wiley, New York (1951).
2. Fischer, F., and Tropsch, H., Brennst.-Chem. 7, 97 (1926).
3. Bell, A. T., Cat. Rev.-Sci. Eng. 23, in press.
4. Biloen, P., and Sachtler, W. M. H., Adv. Cat., in press.
5. Muetterties, E. L., and Stein, J., Chem. Rev. 80, 479 (1979).
6. Masters, C., Adv. OrganoMet. Chem. 17, 61 (1979).
7. Bell, A. T., and Hair, M. L., "Vibrational Spectroscopies for Adsorbed Species", ACS Symposium Series 137, Washington, D. C. (1980).
8. Ozaki, A., "Isotopic Studies of Heterogeneous Catalysis", Academic Press, New York (1977).
9. King, D. L., J. Cat. 51, 386 (1978).

CHAPTER II

Evidence For H_2/D_2 Isotope Effects on Fischer-Tropsch Synthesis Over Supported Ruthenium Catalysts

ABSTRACT

The effects of using D_2 rather than H_2 during Fischer-Tropsch synthesis were investigated using alumina- and silica-supported Ru catalysts. For the alumina-supported catalysts, the rate of CD_4 formation was 1.4 to 1.6 times faster than the formation of CH_4. A noticeable isotope effect was also observed for higher molecular weight products. The magnitude of the isotope effects observed using the silica-supported catalyst was much smaller than that found using the alumina-supported catalysts. The formation of olefins relative to paraffins was found to be higher when H_2 rather than D_2 was used; independent of the catalyst support. The observed isotope effects are explained in terms of a mechanism for CO hydrogenation, and are shown to arise from a complex combination of the kinetic and equilibrium isotope effects associated with elementary processes occurring on the catalyst surface.

INTRODUCTION

Results from a number of recent studies (1-13) suggest that the catalytic synthesis of CH_4 from CO and H_2 over group VIII metals proceeds via stepwise hydrogenation of atomic carbon, formed upon dissociation of chemisorbed CO. It has also been proposed that the formation of higher molecular weight hydrocarbons is initiated by the addition of a methyl group to a methylene group and that further chain growth occurs by the reaction of methylene groups with adsorbed alkyl groups (14, 15). The alkyl groups then react to form olefins and paraffins via either hydrogen elimination or addition. Consistent with these views of CO hydrogenation, one would expect to observe an isotopic effect if D_2 were used instead of H_2. While several attempts have been made to observe such an effect, the results available thus far have been contradictory. In early studies by Jungers et al. (16, 17), the hydrogenation of CO to CH_4 over Ni was observed to proceed more rapidly with D_2 than H_2 and the activation energy was lower for D_2. Recent studies by Mori et al. (18) have confirmed this observation and indicate that methanation over Ni is 1.4 times faster with D_2 than with H_2. Sakharov and Dokukina (19) also observed an inverse isotope effect for a Co/ThO_2/Kieselguhr catalyst. For temperatures between 449 and 466K they found that the formation of CD_4 was 1.2 to 1.5 times faster than the formation of CH_4. A normal isotope effect was observed by McKee (20) for CH_4 synthesis over Ru powder. The ratio of CH_4 to CD_4 formation was 2.2 over the temperature range of 298 to 423K. In contrast to these results, Dalla Betta and Shelef (20,21) reported that no isotopic effect could be discerned for either CH_4 or total hydrocarbon formation over Ni/ZrO_2, Ru/Al_2O_3, or Pt/Al_2O_3 for temperatures between 423 and 498K. Based on this evidence it was suggested that CO dissociation is likely to be the rate-determining step in CO hydrogenation. In a comment on these results, Wilson (23) noted that the overall isotope effect could arise from a combination of kinetic and equilibrium isotope effects, the former favoring the reaction of H_2 and the latter favoring the reaction of D_2. As a result of this, he concluded that the presence or absence of an isotope effect cannot be used to identify the rate determining step.

The present study was undertaken to reexamine the nature of the H_2/D_2 isotope effect associated with the synthesis of CH_4 and higher molecular weight hydrocarbons over silica- and alumina-supported Ru. These investigations were carried out at 1 and 10 atm in the temperature interval of 453 to 548K. An inverse isotope effect was observed for the alumina-supported catalysts, which was largest for CH_4 and declined with increasing carbon number. The magnitude of the inverse isotope effect observed using the silica-supported catalyst was much smaller, and a normal isotope effect was observed for some of the products. A small normal isotope effect on the olefin to paraffin ratio was observed over both catalysts. The significance of these observations is discussed in the light of a proposed mechanism for the hydrogenation of CO over Ru.

EXPERIMENTAL

Catalysts

Two alumina-supported catalysts and one silica-supported catalyst were prepared using Kaiser KA-201 γ-alumina and Davison 70 silica gel as the supports. A 3.0% Ru/Al_2O_3 and a 1.2% Ru/SiO_2 catalyst were prepared by incipient wetness impregnation of the support with an aqueous solution of $RuCl_3$, acidified to pH = 2 to suppress hydrolysis. The resulting slurry was air-dried, and then heated slowly in vacuum from 298 to 423K. Reduction of the chloride was carried out in flowing H_2. The temperature was raised slowly from 298 to 673K and then maintained at 673K for 8 hr.

A second alumina-supported catalyst was prepared by adsorption of $Ru_6C(CO)_{17}$ from a pentane solution under oxygen and moisture free conditions. Synthesis of the cluster complex and details of the impregnation procedure have been described previously (24). Once dried this catalyst, designated as 1.0% Ru_6/Al_2O_3, was reduced in flowing H_2 under conditions identical to those used to reduce the catalysts prepared from $RuCl_3$.

The dispersion of the 1.0% Ru_6/Al_2O_3 and the 3.0% Ru/Al_2O_3 catalysts, measured by H_2 chemisorption, were found to be 1.0 and 0.5, respectively. The dispersion of the 1.2% Ru/SiO_2 catalyst could not be determined by this technique since a reproducible determination of H_2 uptake could not be obtained. As a result, the dispersion of this catalyst was measured by CO chemisorpton and determined to be 0.25, based on the assumption that the ratio of CO to surface Ru atoms is unity. The validity of this assumption is supported by previous studies with low dispersion Ru/Al_2O_3 catalysts (25) and by the observation that infrared spectra of CO adsorbed on the Ru/SiO_2 used in this study (7,26) show only a single band, attributable to linearly adsorbed CO.

All reactions were carried out using a premixed feed composed of H_2 or D_2 and CO at a ratio of $H_2(D_2)/CO = 3.0$. The feed mixtures were blended in small cylinders using pure components. Following filling, the bottom of the cylinder containing the mixture was heated for one day to assure uniform gas mixing. The blended mixture was then analyzed by gas chromatography to establish the concentration of CO. If the original mixture was not correct, additional CO or H_2 (D_2) was added. By following this procedure, it was possible to obtain mixtures containing 25 ± 0.5% CO.

Procedure

Rate data were obtained using a stainless steel microreactor heated in a fluidized bed. The reaction products were analyzed using an on-line gas chromatograph fitted with balanced 2.4 mm by 1 m columns packed with Chromosorb 106. The column oven was temperature programmed from 318 to 503K at 10K/min, and the hydrocarbon products were detected by a flame ionization detector. Calibration of the chromatograph was carried out using mixtures containing known concentrations of the products. In addition, by injecting pure samples of CH_4 and CD_4 it was established that the detector sensitivities for deuterated and hydrogenated products were identical.

Each experiment with a fresh catalyst charge [30 mg for the 3.0% Ru/Al_2O_3 catalyst and 100 mg for the 1.0% Ru_6/Al_2O_3 and the 1.2%

Ru/SiO_2 catalysts was initiated by a 10 to 12 hr reduction in flowing H_2 at 673K and 10 atm. The temperature was then lowered to 498K and the feed mixture was introduced at a flow rate of 200 cm^3/min (NTP). Ten minutes after the reaction began, a gas sample was taken for analysis and the gas feed was switched over to pure H_2 for 1 hr. By alternating short reaction periods and longer reduction periods, a stable catalyst activity could be achieved after several cycles. Once this status was attained, the catalyst was cooled to 453K and data were taken between 453 and 498K. The catalyst was then heated to 548K, and data were taken between 548 and 498K. By following this procedure, a check could be obtained for catalyst deactivation. In all cases the reaction rate measured at 498K could be reproduced to within a few percent. It should be noted further, that in all instances the conversion of CO was low, ranging from 0.02% at 453K to 1.5% at 548K.

RESULTS

Arrhenius plots for the rates of formation of C_1 through C_5 hydrocarbons over Ru_6/Al_2O_3 and Ru/SiO_2 are given in Figs. 1-5. The open points represent turnover numbers measured with H_2 and the solid points represent turnover numbers measured with D_2. The rates of formation of C_2 through C_4 paraffins and olefins have been shown separately in Figs. 2-4. Representation in this fashion was not possible, though, for the C_5 products since the resolution of the chromatographic peaks for olefins and paraffins was inadequate.

The data presented in Fig. 1 show that the production of CD_4 occurs approximately 1.5 times faster than CH_4 over Ru_6/Al_2O_3, both at 1 and 10 atm. At 10 atm the production of CD_4 is also favored over

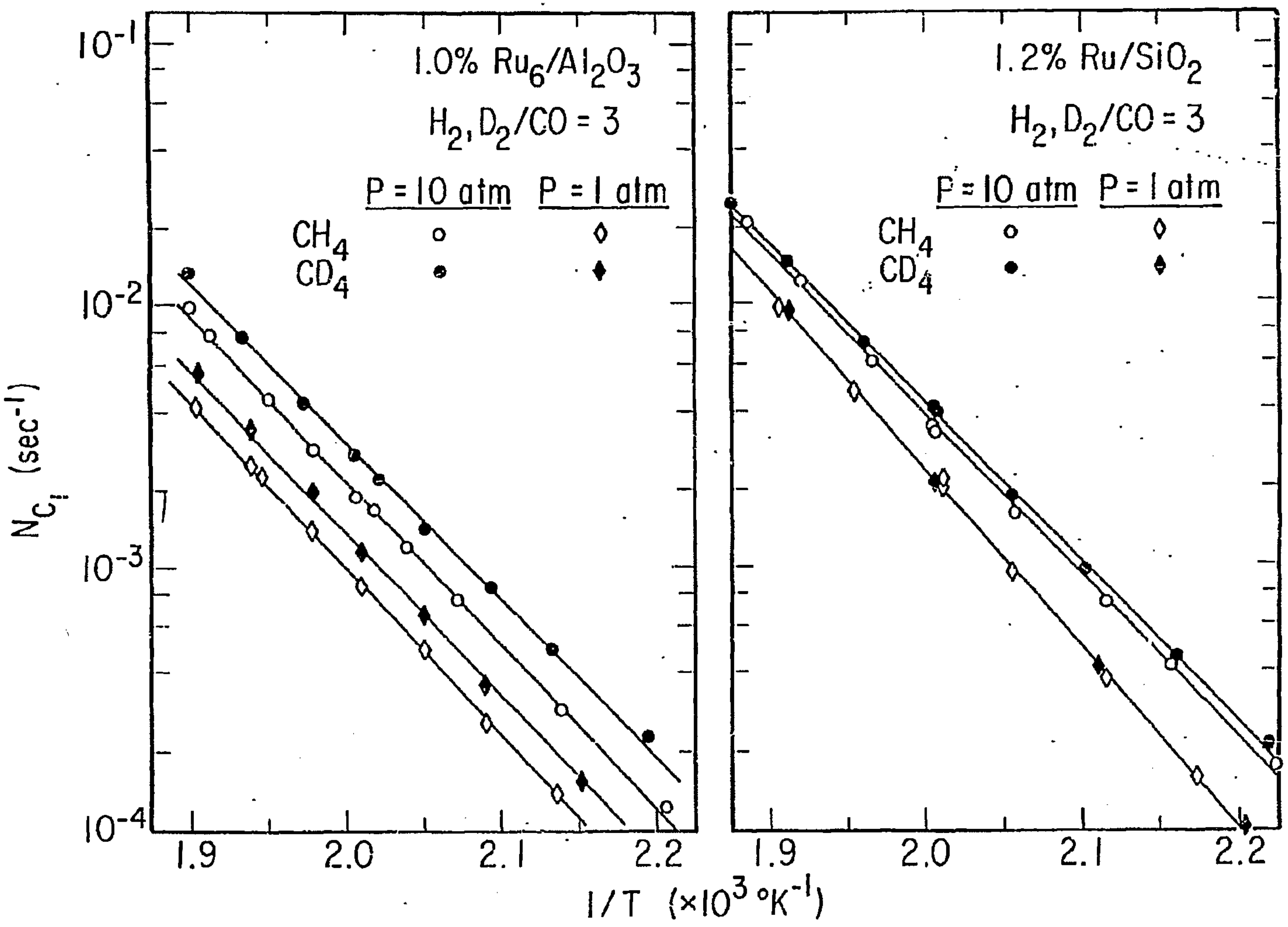

XBL 807-10808

Fig. 1. Arrhenius plots for the formation of methane at 1 and 10 atm.

Ru/SiO_2, but the magnitude of the inverse isotope effect is now 1.1. When the pressure is reduced to 1 atm, no isotope effect can be detected for this catalyst. It is noted further that the activation energy for both CH_4 and CD_4 lies between 27 and 28 Kcal/mole, independent of the total pressure or catalyst composition.

Figures 2-5 show that an inverse isotope effect is also apparent for the production of C_2 through C_5 olefins and paraffins over the alumina-supported catalyst. The upward curvature of the Arrhenius plots for C_2D_6 and C_2H_6 can be explained in the following manner. For temperatures below about 493K, olefins and paraffins are produced by parallel processes as suggested by the fact that the feed flow rate does not alter the olefin to paraffin ratio of the products. At higher temperatures, hydrogenation of the olefin takes place. The presence of this secondary reaction is confirmed by observing an increase in the olefin to paraffin ratio with increasing feed flow rate. When partial hydrogenation of the olefin product does occur, the Arrhenius plot curves upwards, since the paraffin is now produced via two pathways.

Examination of the Arrhenius plots for C_2 through C_5 products formed over the Ru/SiO_2 catalyst show that the isotope effects are significantly different from those observed using the alumina-supported catalyst. Normal isotope effects are seen for the C_2 and C_4 products but no significant isotope effect is found for the C_3 or C_5 products. Here again, the upwards curvature in the Arrhenius plots for the C_2 through C_4 paraffins at higher temperatures can be ascribed to partial hydrogenation of the corresponding olefins.

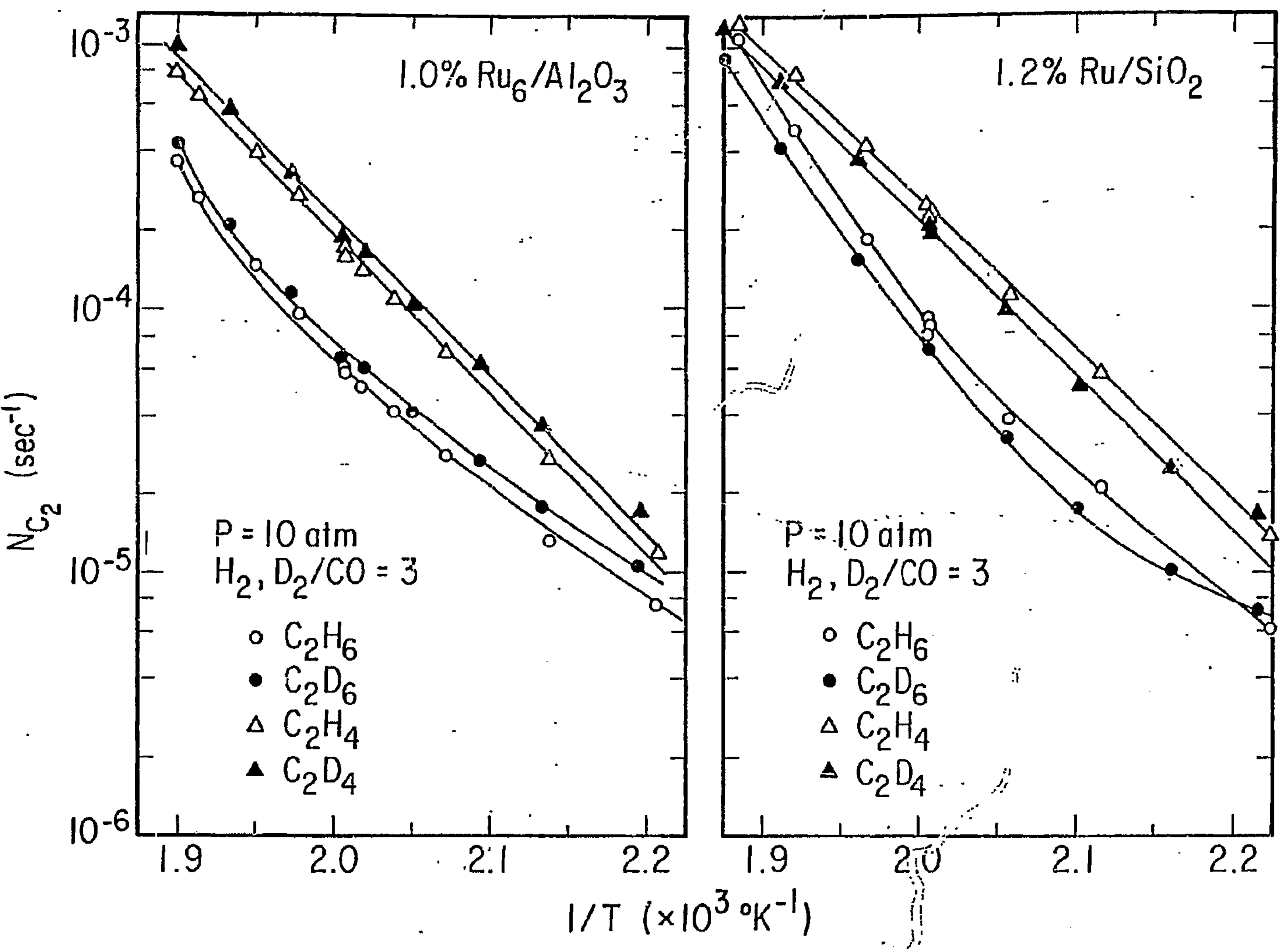

XBL 807-10809

Fig. 2. Arrhenius plots for the formation of ethylene and ethane at 10 atm.

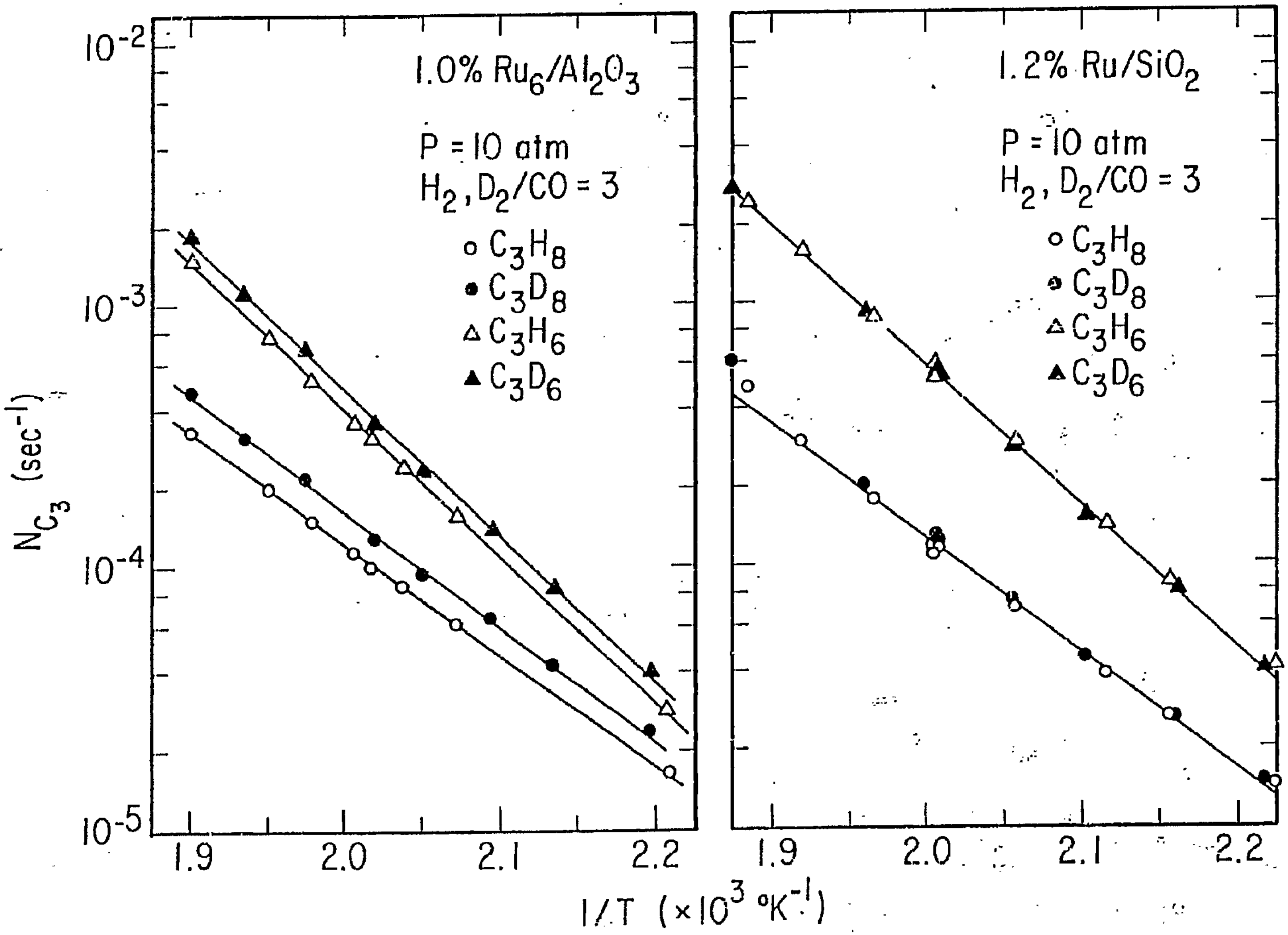

XBL 807-10810

Fig. 3. Arrhenius plots for the formation of propylene and propane at 10 atm.

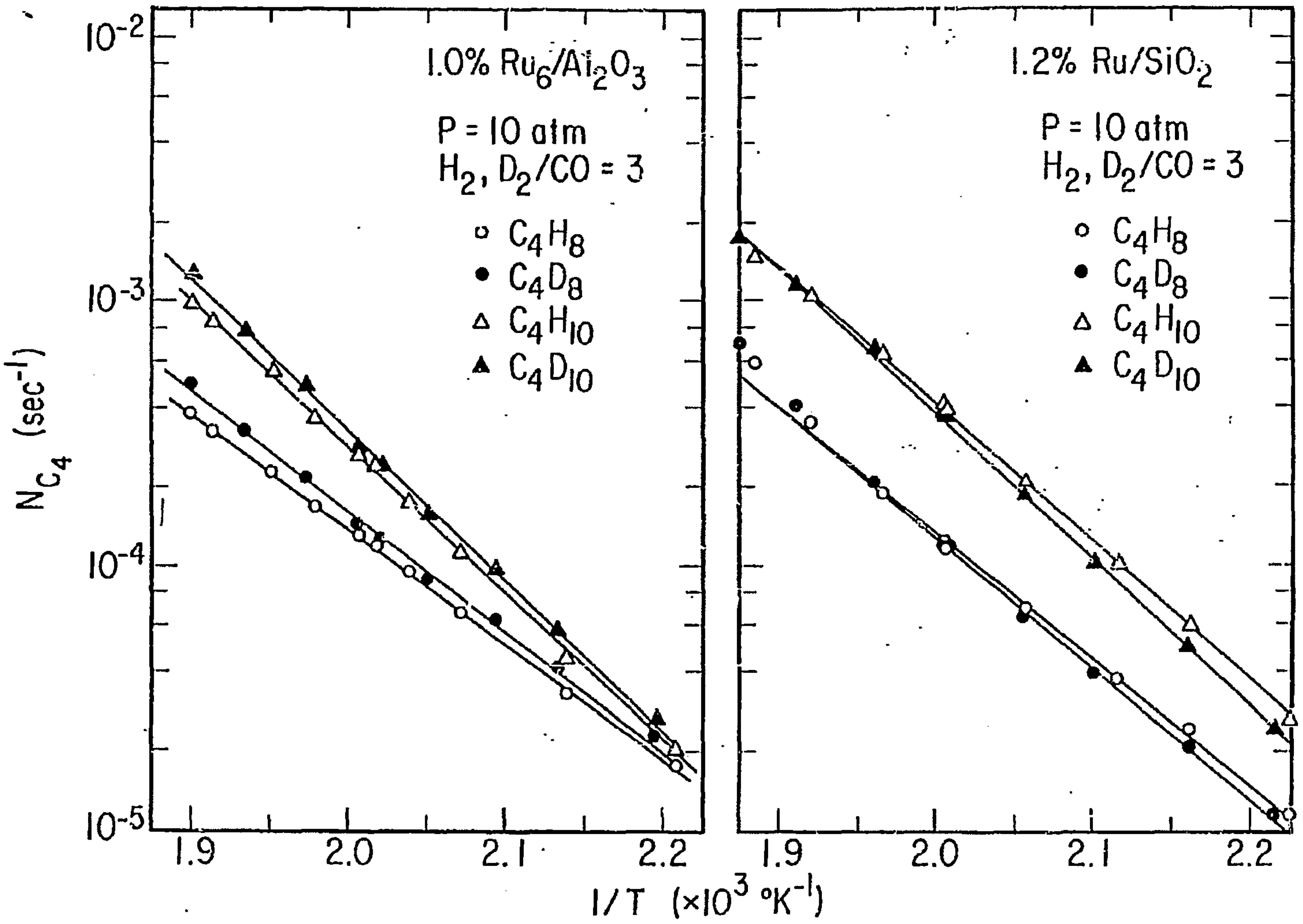

XBL 807-10811

Fig. 4. Arrhenius plots for the formation of butene and butane at 10 atm.

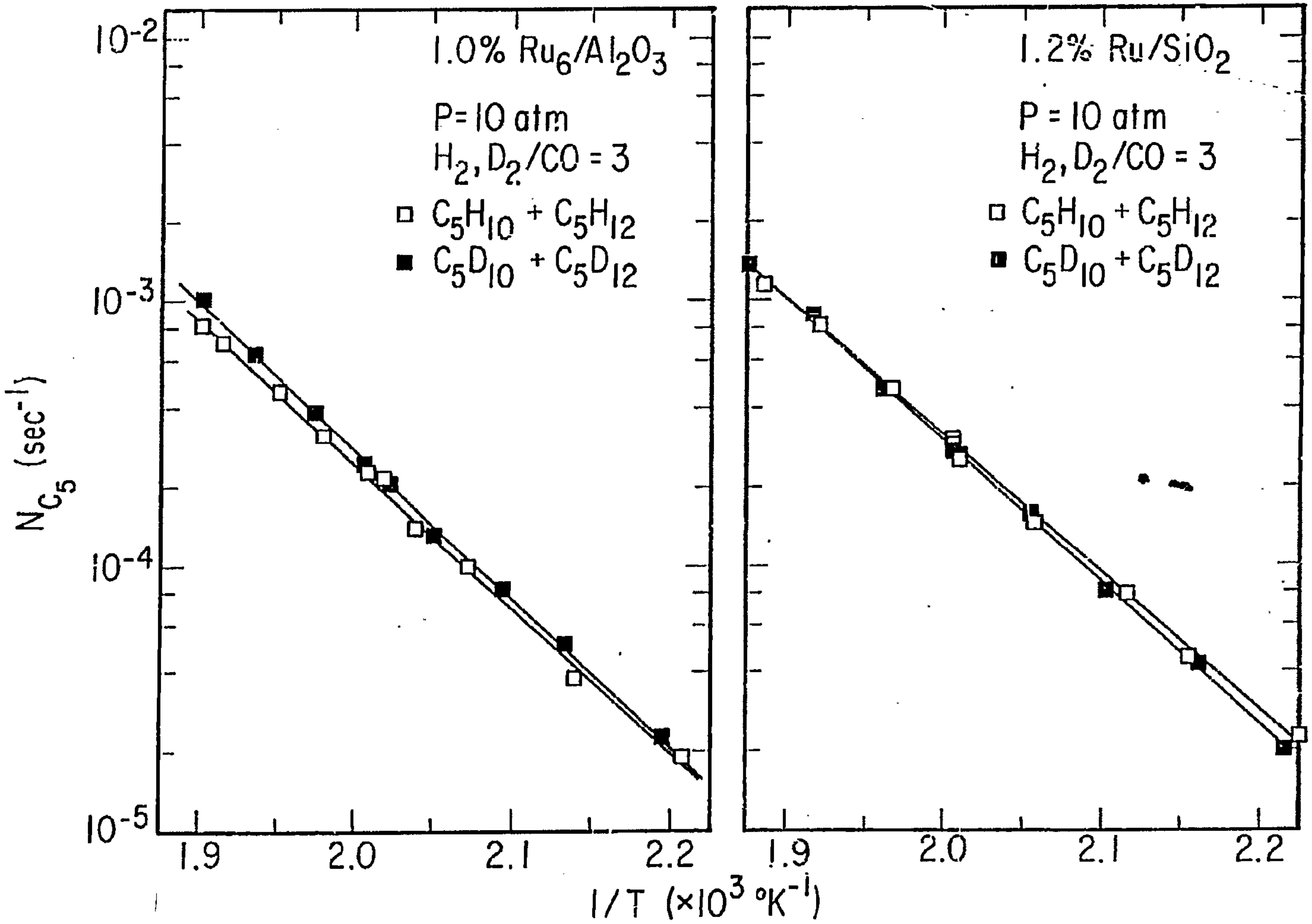

XBL 807-10812

Fig. 5. Arrhenius plots for the formation of pentene and pentane at 10 atm.

Experiments identical to those shown in Figs. 2-5 were also carried out at 1 atm. The isotope effects for the alumina-supported catalyst were similar to those observed at 10 atm. Virtually no isotope effect was observed, though, for the silica-supported catalyst.

To determine whether the manner of preparation of the alumina-supported catalyst altered the nature or magnitude of the isotope effect, experiments were conducted with the Ru/Al_2O_3 catalyst prepared by reduction of $RuCl_3$. A comparison of the isotope effects for C_1 through C_5 hydrocarbons observed over the catalysts prepared from $Ru_6C(CO)_{17}$ and $RuCl_3$ is given in Table I. It is seen that the isotope effects are virtually the same for the two catalysts. As a consequence, it seems appropriate to ascribe the observed isotope effects to the nature of the interactions between ruthenium and alumina rather than to the origin of the ruthenium.

The results presented in Table I indicate further that the magnitude of the isotope effect declines as the number of carbon atoms in the product increases. This trend is shown even more clearly in Fig. 6. Quite interestingly, for $n > 5$ the isotope effect becomes less than unity, indicating a slightly faster product formation rate with H_2 than with D_2.

The effects of temperature on the olefin to paraffin ratio are shown in Figs. 7-9. For each catalyst, the ratio is observed to pass through a maximum with increasing temperature. The position of the maximum defines the temperature above which hydrogenation of the olefin becomes significant. For all three products the olefin to paraffin ratio is higher when the silica-supported catalyst is used, but the

Table I. Comparison of the H_2/D_2 Isotope Effects for 1.0% Ru_6/Al_2O_3 and 3.0% Ru/Al_2O_3.

	455K		475K		500K	
	Ru_6/Al_2O_3	Ru/Al_2O_3	Ru_6/Al_2O_3	Ru/Al_2O_3	Ru_6/Al_2O_3	Ru/Al_2O_3
$N^D_{C_1}/N^H_{C_1}$	1.57	1.61	1.49	1.56	1.40	1.52
$N^D_{C_2}/N^H_{C_2}$	1.22	1.18	1.19	1.16	1.16	1.14
$N^D_{C_3}/N^H_{C_3}$	1.17	1.19	1.19	1.21	1.23	1.22
$N^D_{C_4}/N^H_{C_4}$	1.08	1.08	1.12	1.13	1.15	1.18
$N^D_{C_5}/N^H_{C_5}$	1.05	1.05	1.07	1.08	1.12	1.12

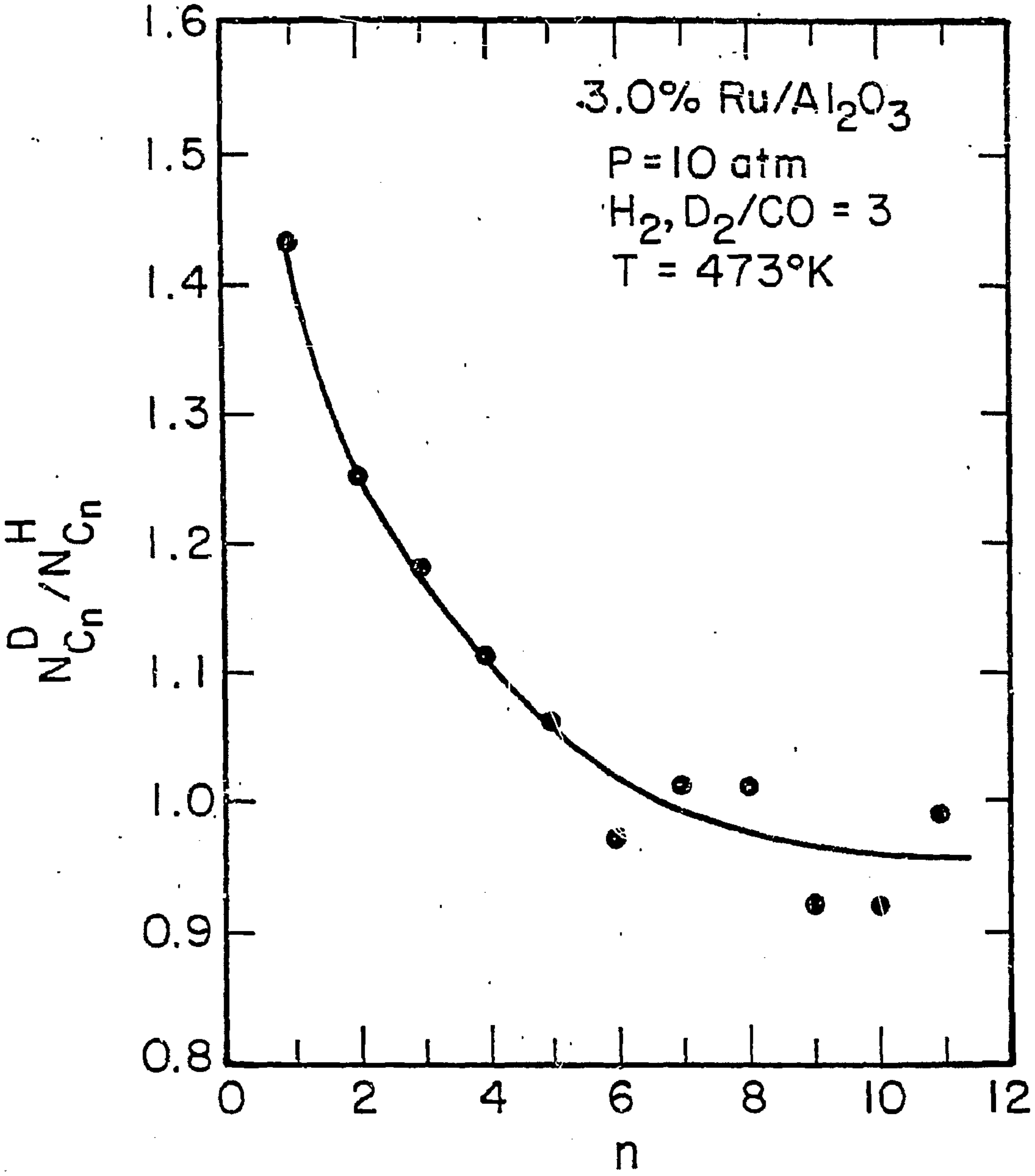

XBL 807-10813

Fig. 6. Dependence of the isotope effect on the number of carbon atoms in the product.

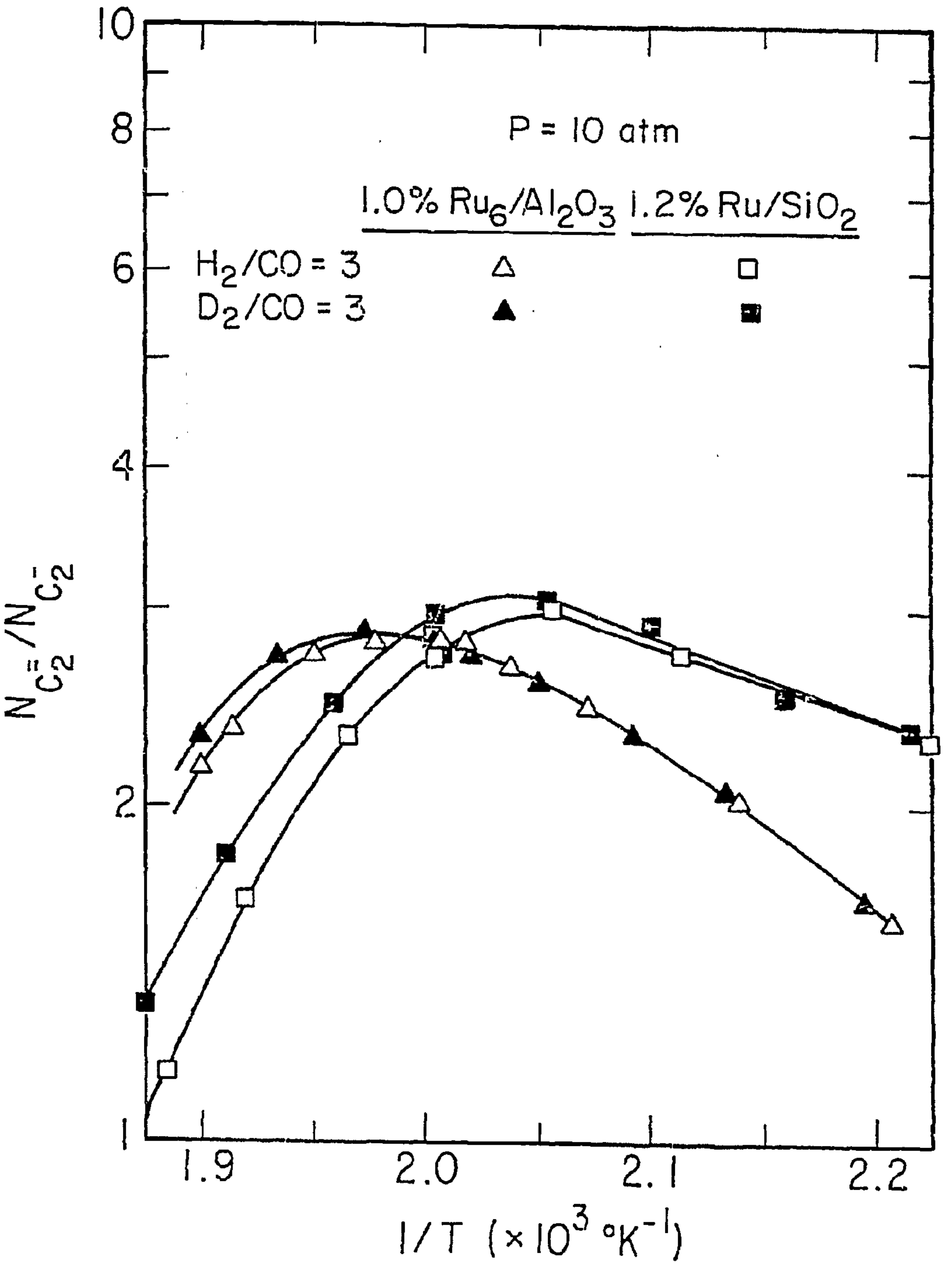

XBL 807-10814

Fig. 7. Dependence of the olefin to paraffin ratio for C_2 products on the inverse temperature.

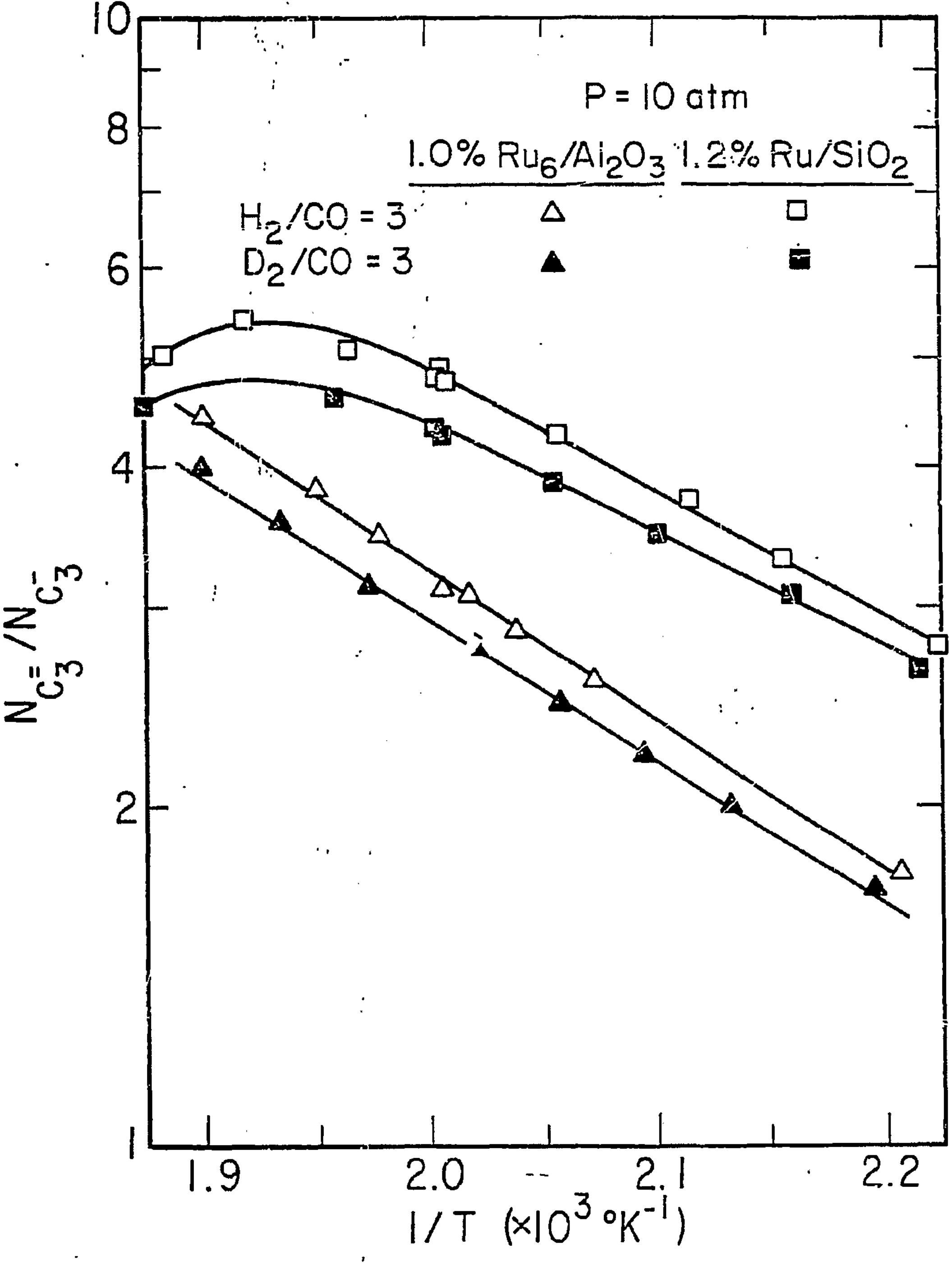

XBL 807-10815

Fig. 8. Dependence of the olefin to paraffin ratio for C_3 products on the inverse temperature.

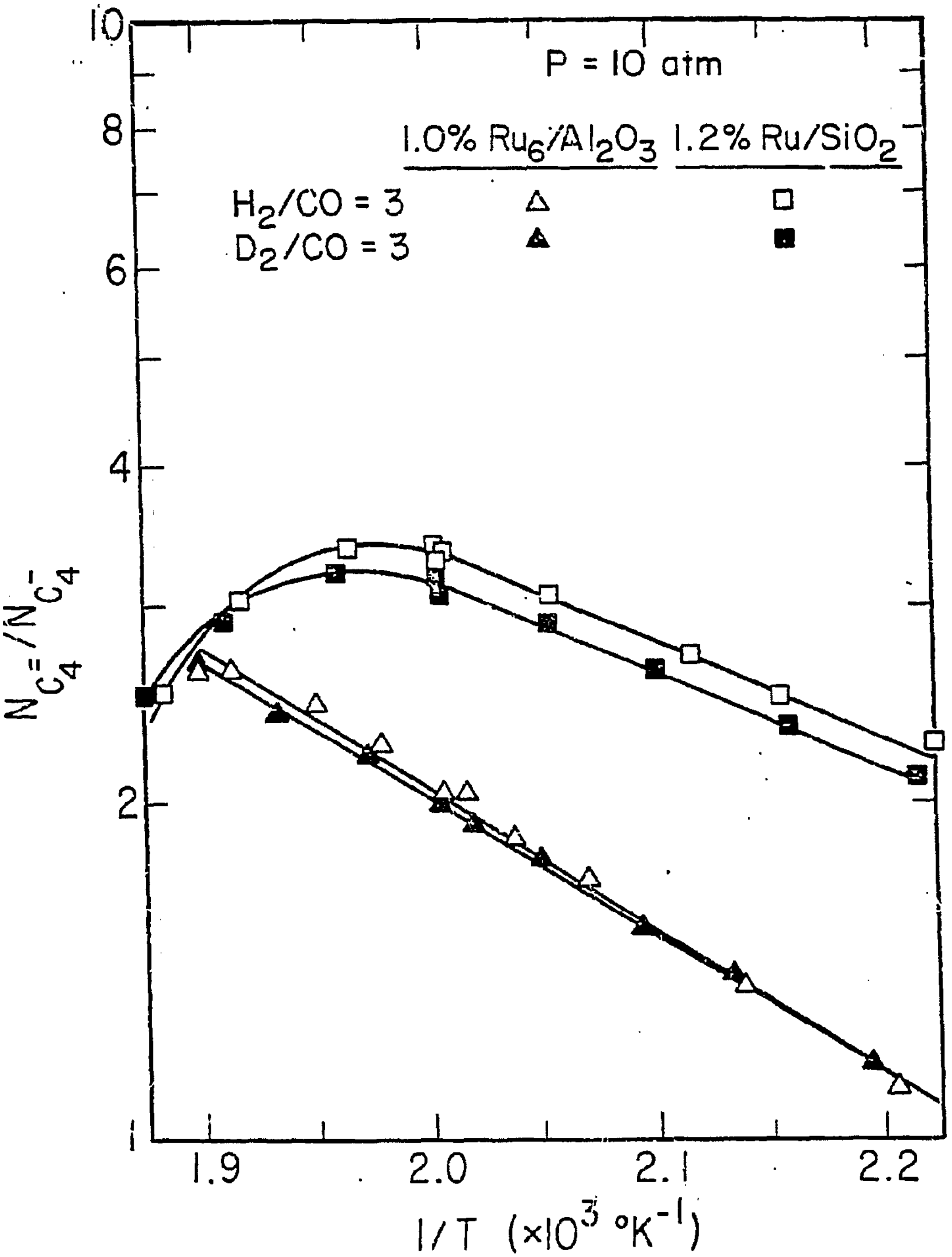

XBL 807-10816

Fig. 9 Dependence of the olefin to paraffin ratio for C_4 products on the inverse temperature.

temperature at which olefin hydrogenation becomes significant is higher for the alumina-supported catalyst. While the use of D_2 instead of H_2 does not influence the general characteristics of the olefin to paraffin ratio dependence on temperature, a number of subtle effects are apparent. For the alumina-supported catalyst, there is virtually no isotope effect on the olefin to paraffin ratios for C_2 and C_4 products. However, the ratio of propylene to propane is definitely higher when H_2 rather than D_2 is present in the feed. For the silica-supported catalyst, no isotope effect is detectable for the C_2 products at temperatures below 500K. Above this temperature, though, the ethylene to ethane ratio is higher in the presence of D_2. By contrast, the olefin to paraffin ratios for the C_3 and C_4 products are higher in the presence of H_2 over the whole temperature range. The olefin to paraffin ratio was also examined for the data obtained at 1 atm. In this case the olefin to paraffin ratios were approximately three fold higher than those shown in Figs. 7-9 and higher values were obtained with H_2 than with D_2 for all three products over both catalyst.

DISCUSSION

The data presented here clearly show that an inverse isotope effect can be observed for the formation of CH_4 over Ru catalysts. The magnitude of the effect is 1.6-1.4 for the alumina-supported catalysts, both at 1 and 10 atm. For silica-supported Ru the effect is 1.1 at 10 atm but drops to 1.0 at 1 atm. These results contradict the conclusion of Dalla Betta and Shelef (21) that there is no isotope effect for methane formation over Ru. Since the weight loading and dispersion of the catalyst used by Dalla Betta and Shelef were similar to that of the

Ru_6/Al_2O_3 catalyst used in this work, it is difficult to understand why these authors did not observe an isotope effect. One possibility may be that an insufficient amount of data were taken, particularly with D_2. The present results also differ from those obtained by McKee (20). It should be noted, though, that comparison in this case may not be appropriate since McKee's studies were conducted with Ru powder at much lower pressures (60 Torr CO and 60 Torr H_2) and temperatures (298 to 423K) than those used here. Furthermore, as was noted by Dalla Betta and Shelef (21), the analytical procedure used by McKee may not have been free of error. Products were detected by a mass spectrometer connected to the reaction chamber by a molecular leak. Since this method of sampling can give rise to different sensitivities for CH_4 and CD_4, and since calibration of the mass spectrometer was not discussed, it is not possible to know whether the reported results are accurate.

An interpretation of the isotope effects observed in the present study can be developed by consideration of the following reaction network:

1. $CO + S \rightleftarrows CO_s$
2. $CO_s + S \rightleftarrows C_s + O_s$
3. $H_2 + 2S \rightleftarrows 2H_s$
4. $H_2 + O_s \rightleftarrows H_2O + S$
5. $C_s + H_s \rightleftarrows CH_s + S$
6. $CH_s + H_s \rightleftarrows CH_{2s} + S$
7. $CH_{2s} + H_s \rightleftarrows CH_{3s} + S$
8. $CH_{3s} + H_s \rightarrow CH_4 + 2S$

9. $CH_{3s} + CH_{2s} \rightarrow C_2H_{5s} + S$

10. $C_2H_{5s} + S \rightarrow C_2H_4 + H_s + S$

11. $C_2H_{5s} + H_s \rightarrow C_2H_6 + 2S$

12. $C_2H_{5s} + CH_{2s} \rightarrow C_3H_{7s} + S$

etc.

This mechanism is supported by a significant number of recent investigations (1-15) and has been discussed in detail by Bell (27). As a result, no attempts will be made here to justify the elementary steps included.

Overall rate expressions for the formation of methane can be derived from the proposed scheme provided a number of simplifying assumptions are invoked. The first is that the Ru surface is nearly saturated by adsorbed CO. This assumption is supported by in situ infrared observations carried out both at low and high pressure (7,26,28,29). The second assumption is that water is the primary product through which oxygen is removed from the catalyst surface. Here, too, the assumption is substantiated by experimental evidence (7,26). The third assumption is that all of the steps indicated as being reversible are, in fact, at equilibrium. No substantiation of this assumption is currently possible.

Two limiting forms can be obtained for the kinetics of methane formation, depending upon whether methanation or the synthesis of higher molecular weight hydrocarbons is dominant (26,27). In the former case, the rate of methane formation is given by

$$N_{C_1} = k_e\, P_{H_2}^{1.5}/P_{CO} \tag{1}$$

$$k_e = \frac{K_3}{K_1}\,(k_4 k_8 K_5 K_6 K_7)^{1/2} \tag{2}$$

where k_i and K_i are the rate coefficient and equilibrium constant, respectively, for the i^{th} elementary reaction. In the latter case, the rate is given by

$$N_{C_1} = k_e\, P_{H_2}^{1.5}/P_{CO}^{1.33} \tag{3}$$

$$k_e = k_8 \left[\frac{k_4 K_2 K_3^{3.5} K_5 K_6 K_7^2 \quad (1-\alpha)}{k_p K_1^4}\right]^{1/3} \tag{4}$$

where k_p is the rate coefficient for the addition of CH_2 groups to adsorbed alkyls (i.e. reactions 9, 12, etc.) and α is the probability of chain propagation (30). With the exception of studies conducted at pressures of 1 atm or less, using H_2 to CO ratios greater than three, neither of the limiting assumptions is strictly valid. However, recent experimental studies by Kellner and Bell (26) have shown that for pressures between 1 and 10 atm and H_2/CO ratios between 1 and 3 the kinetics of methane formation can be described empirically by the expression $N_{C_1} = k_e P_{H_2}^{1.4}/P_{CO}$, in good agreement with Eqn. 1.

The forms of Eqns. 1 and 3 indicate that the effective rate coefficient for methane synthesis is a complex product of rate coefficients and equilibrium constants. As a consequence, the observed isotope effect must result from the combination of kinetic and equilibrium isotope effects, as suggested by Wilson (23). To further pursue the influence of these two effects, it is useful to recall that rate coefficients and equilibrium constants can be expressed in the formalism of statistical mechanics (31). Thus,

$$K = \frac{kT}{h} \frac{q^{\ddagger}}{\prod_{i} q_r^{\nu_i}} \qquad (5)$$

$$K = \frac{\prod_{i} q_p^{\nu_j}}{\prod_{i} q_r^{\nu_i}} \qquad (6)$$

where (kT/h) is a frequency factor; q_r, q_p, and $q^{\ddagger}$ are the partition functions for reactants, products, and transition state complexes; and ν_i and ν_j are the stoichiometric coefficients for reactant i and product j. Changes in the magnitudes of k and K due to isotopic substitution result from the influences of molecular mass on the molecular partition functions. In most instances, the largest portion of the isotope effect arises from changes in the ground state vibrational frequencies.

Ozaki (32) has noted that the differences in the ground state vibrational frequencies of deuterated and hydrogenated species usually lead to the conclusion that the equilibrium constant for addition of deuterium to an adsorbed species is larger than that for the addition of hydrogen. An example of this generalization which is relevant to the present discussion has been reported recently by Calvert et al. (33). In this work it was shown that deuterium is preferentially incorporated into methyl and methylene ligands present in triosmium complexes. The equilibrium constant for the reaction $Os_3(CO)_{10}CH_2D_2 \rightleftarrows Os_3(CO)_{10}CD_2H_2$ was determined to be 2.50 and that for the reaction $Os_3(CO)_{10}(CH_2D)D \rightleftarrows Os_3(CO)_{10}(CD_2H)H$ was found to be 1.74. Based on this evidence, one would suspect that the product $K_5K_6K_7$, appearing in Eqns. 1 and 3, should be significantly larger when D_2 is involved in steps 5 through 7 rather than H_2.

The equilibrium isotope effect for $H_2(D_2)$ chemisorption, reaction 3, can be examined explicitly. If it is assumed that the adsorbed atoms are immobile but have three degrees of vibrational freedom, then it can readily be shown that

$$\frac{K_3^D}{K_3^H} = \left(\frac{m_{H_2}}{m_{D_2}}\right)^{5/2} \exp\left\{\left[-2\sum_{i=1}^{3}(\nu_i^D - \nu_i^H) + (\nu_1^{D2} - \nu_1^{H2})\right] h/2kT\right\} \qquad (7)$$

where m_{H_2} and m_{D_2} are the masses of H_2 and D_2, ν_i^H and ν_i^D are the vibrational frequencies for adsorbed H and D atoms, and ν_1^{H2} and ν_1^{D2} are the vibrational frequencies for gaseous H_2 and D_2. Evaluation of K_3^D/K_3^H using the values of the vibrational frequencies given in Table II shows that this ratio lies between 0.79 and 0.62 for temperatures between 453 and 543K. It is significant to note that while $K_3^D/K_3^H < 1$ over the temperature range of interest in these studies, the argument of the exponential factor in Eqn. 7 leads to the expectation that the heat of adsorption for D_2 on Ru should be 1.34 Kcal/mole larger than that for H_2. These conclusions are consistent with experimental observations on Ni.

Table II. Vibrational Frequencies for Molecular and Atomically Adsorbed H_2 and D_2.

Species	Mode	Frequency (cm^{-1}) (a)
H_2	ν (H-H)	4161
D_2	ν (D-D)	2993
M-H	ν (M-H)	2250-1700
	δ (M-H) (b)	800-600
M-D	ν (M-D)	1591-1202
	δ (M-D) (b)	566-424

(a) Taken from ref. (35)

(b) Doubly degenerate

By means of calorimetric measurements on a Ni film, Wedler et al. (34) determined that the heat of adsorption of D_2 was about 1 Kcal/mole larger than that for H_2. The displacement of adsorbed H atoms by D_2 and of adsorbed D atoms by H_2 on Ni catalysts was investigated by Gundry (35). His results showed that the apparent equilibrium constant for displacement, which is equivalent to K_3^D/K_3^H, varied from 2.4 at 178K to near unity at 273K. Based on this variation with temperature, it was estimated that the heat of adsorption of D_2 was 0.60 Kcal/mole greater than that for H_2. The stronger adsorption of D_2 has also been confirmed by Wedler and Stanelmann (36) on a Ni film. Extrapolation of Gundry's results to the temperature levels used in this study would also lead to the conclusion that $K_3^D/K_3^H < 1$.

The kinetic isotope effect for reactions involving the addition of hydrogen has also been considered by Ozaki (32). Here again, he concludes that differences in the vibrational frequencies of deuterated and hydrogenated species are the primary origin of the effect and that in most cases $k_H > k_D$. For reactions involving a molecule of H_2 or D_2, and an adsorbed species (i.e., reaction 4), the ratio of masses arising from the transitional and rotational portions of the partition functions of H_2 and D_2 only serve to further increase the magnitude of the kinetic isotope effect.

Based upon the factors just considered, it is clear that the overall isotope effect on methane formation results from a complex combination of kinetic and equilibrium effects. Since the magnitude of these individual effects cannot be predicted reliably, it is not possible to conclude whether the observed isotope effect is consistent with the structure of the effective rate coefficient appearing in Eqns. 1 and 3. What is evident, though, is that small changes in the isotope effects associated with individual elementary processes will alter the overall isotope effect. Such changes could arise from modifications of the metal dispersion and/or interaction with the support and might explain why the isotope effect is substantially smaller for the silica-supported catalyst than for either of the alumina-supported catalysts.

The data presented in Fig. 6, show that the magnitude of the inverse isotope effect decreases with increasing carbon number. This pattern can be understood in the following fashion. If it is assumed that the probability of chain propagation, α , is independent of chain length, n, then the rate of formation of hydrocarbons containing n atoms can be expressed as

$$N_{C_n} = (k_{to}\theta_v + k_{tp}\theta_H)\, \alpha^{n-1}\, \theta_{CH_3} \tag{8}$$

$$= (1 + \frac{k_{to}\theta_v}{k_{tp}\theta_H})\alpha^{n-1}\, k_{tp}\theta_H\theta_{CH_3} \tag{9}$$

where k_{to} and k_{tp} are the rate coefficients for termination of chain growth by formation of olefins and paraffins (i.e. reactions 10 and 11), θ_v is the fraction of the catalyst surface that is vacant, and θ_H and θ_{CH_3} are the fractions of the surface covered by H atoms and CH_3 groups. The second term in the parenthesis of Eqn. 9 can be rewritten as

$$\frac{k_{to}\theta_v}{k_{tp}\theta_H} = \frac{k_{to}}{k_{tp}K_3^{1/2}P_{H_2}^{1/2}} \tag{10}$$

$$= \beta/P_{H_2}^{1/2} \tag{11}$$

The magnitude of the isotope effect for any value of n can now be expressed by taking the ratio of the rate in the presence of D_2, $N^D_{C_n}$, to that in the presence of H_2, $N^H_{C_n}$. Combining Eqns 9 and 11 with the expression $N_{C_1} = k_8\theta_H\theta_{CH_3}$, we obtain.

$$\frac{N^D_{C_n}}{N^H_{C_n}} = \frac{k^D_{tp}}{k^H_{tp}}\;\frac{k^H_8}{k^D_8}\;\frac{(1 + \beta^D/P_{D_2}^{1/2})}{(1 + \beta^H/P_{H_2}^{1/2})}\left(\frac{\alpha^D}{\alpha^H}\right)^{n-1}\frac{N^D_{C_1}}{N^H_{C_1}} \tag{12}$$

The form of Eqn. 12 suggests that the isotope effect for any carbon number can be related to that observed for methane. To account for the decrease in $N^D_{C_n}/N^H_{C_n}$ with n it must be concluded that $\alpha^D < \alpha^H$. It is also noted that Eqn. 12 predicts that for a sufficiently large value of n, $N^D_{C_n}/N^H_{C_n}$ could become less than one. While there is considerable amount of scatter in the data for $n > 5$ shown in Fig. 6, it does appear that the isotope effect eventually becomes smaller than unity.

The influence of H_2 and D_2 on the olefin to paraffin ratio can also be understood in the context of the present discussion. The proposed reaction mechanism leads to the following expression for the olefin to paraffin ratio:

$$\frac{N_{C_n^=}}{N_{C_n^-}} = \frac{k_{to}}{k_{tp}K_3^{1/2}P_{H_2}^{1/2}} \tag{13}$$

$$= \beta/P_{H_2}^{1/2}$$

This expression is found to be in good agreement with experimental data taken by Kellner and Bell (26) for temperatures below which olefin hydrogenation is not significant. The form of Eqn. 13 again indicates that both kinetic and equilibrium isotope effects will influence the olefin to paraffin ratio. Since it has already been shown that $K_3^D < K_3^H$, the observation of a normal isotope effect on the olefin to paraffin ratio implies that $(k_{to}^D/k_{tp}^D) < (k_{to}^H/k_{tp}^H)$ or alternatively that $(k_{tp}^D/k_{tp}^H) > (k_{to}^D/k_{to}^H)$.

CONCLUSIONS

The results of the present investigation have shown that an inverse isotope effect can be observed during the synthesis of CH_4 over silica- and alumina-supported Ru catalysts, and that the magnitude of the effect is larger for alumina-supported catalysts.

Noticeable isotope effects have also been observed during the synthesis of C_2 through C_{11} olefins and paraffins. For C_2 through C_5 hydrocarbons, synthesis over an alumina-supported catalyst occurs more rapidly in the presence of D_2 rather than H_2, but the magnitude of the inverse isotope effect declines towards unity with increasing number of carbon atoms in the product. The synthesis of C_6 through C_{11} hydrocarbons appears to be favored by H_2, and, thus, a normal isotope effect is observed for these products.

The olefin to paraffin ratio of the products also depends on whether D_2 or H_2 is the reactant. Olefin formation is favored with H_2 over both silica- and alumina-supported catalysts.

The observed isotope effects can be rationalized on the basis of a mechanism proposed to describe the formation of CH_4 and higher molecular weight products. Rate expressions derived from this mechanism lead to the conclusion that the overall isotope effect results from a combination of the kinetic and equilibrium isotope effects associated with individual elementary steps. The proposed mechanism also provides explanations for the decline in the magnitude of the inverse isotope effect with increasing product carbon number and the higher olefin to paraffin ratio observed when using H_2.

REFERENCES

1. Wentrcek, P. R., Wood, B. J., and Wise, H., J. Catal. 43, 363 (1976).

2. Araki, M., and Ponec, V., J. Catal. 44, 439 (1976).

3. Sexton, B. A., and Somorjai, G. A., J. Catal. 46, 167 (1977).

4. Rabo, J. A., Risch, A. P., and Poutsma, M. L., J. Catal. 53, 295 (1978).

5. Sachtler, J. W. A., Kool, J. M., and Ponec, V., J. Catal. 56, 284 (1979).

6. Low, G. G., and Bell, A. T., J. Catal. 57, 397 (1979).

7. Ekerdt, J. G., and Bell, A. T., J. Catal. 58, 170 (1979).

8. McCarty, J. G., and Wise, H., Chem. Phys. Letters 61, 323 (1979).

9. Krebs, H. J., Bonzel, H. P., and Gafner, G., Surf. Sci. 88, 269 (1979).

10. Goodman, D. W., and White, J. M., Surf, Sci 90, 201 (1979).

11. Bonzel, H. P., and Krebs, H. J., Surf. Sci. 91, 499 (1980).

12. Bonzel, H. P., and Krebs, H. J., ACS Div. Fuel Chem. Prepr. 25(2), 18, (1980).

13. Kelley, R. D., Goodman, D. W., and Madey, T. E., ACS Div. Fuel Chem. Prepr. 25(2), 43 (1980).

14. Biloen, P., Helle, J., and Sachtler, W. M. H., J. Catal. 58, 95 (1979).

15. Ekerdt, J. G., and Bell, A. T., J. Catal., 62, 19 (1980).

16. Luytens, L., and Jungers, J. C., Bull. Soc. Chim. Belg. 54, 303 (1945).

17. Nicolai, J., Hont, M., and Jungers, J. C., Bull. Soc. Chim. Belg. 55, 160 (1946).

18. Mori, T., Masuda, H., Imai, H., Miyamoto, A., and Murakami, Y., Shokubai, 22, 7 (1980).

19. Sakharov, M. M. and Dokukina, E. S., Kinet. i Kataliz 2, 710 (1961).

20. McKee, D. W., J. Catal. 8, 240 (1967).

21. Dalla Betta, R. A., and Shelef, M., J. Catal. 49, 383 (1977).

22. Shelef, M., and Dalla Betta, R. A., J. Catal. 60, 169 (1979).

23. Wilson, T. P., J. Catal. 60, 167 (1979).

24. Kuznetsov, V. L., Bell, A. T., and Yermakov, Yu. I., J. Catal. 65, 374 (1980).

25. Dalla Betta, R. A., J. Phys. Chem. 79, 2519 (1975).

26. Kellner, C. S. and Bell, A. T., to be submitted.

27. Bell, A. T., Catal. Rev. Sci. Eng., in press.

28. Dalla Betta, R. A. and Shelef, M., J. Catal. 48, 111 (1977).

29. King, D. L., J. Catal. 77, 61 (1980).

30. Madon, R., J. Catal. 57, 183 (1979).

31. Laidler, K. J., Chemical Kinetics, 2nd ed., McGraw Hill, New York, 1965.

32. Ozaki, A., Isotopic Studies of Heterogeneous Catalysis, Academic Press, New York, 1977.

33. Calvert, R. B., Shapley, J. R., Schultz, A. J., Williams, J. M., Suib, S. L., and Stucky, G. D., J. Am. Chem. Soc. 100, 6240 (1978).

34. Wedler, G., Bröker, F. J., Fisch, G., and Schroll, G., Z. Phys. Chem. N.F. 76, 212 (1971).

35. Gundry, P. M., Proc. 2nd Int. Congr. Catalysis, No. 51, 1083 (1960).

36. Wedler, G., and Stanelmann, G., Ber. Bunsenges. Physik. Chem. 75, 1026 (1971).

37. Nakamoto, K., Infrared Spectra of Inorganic and Coordination Compounds, 3rd ed., Wiley, New York 1978.

Infrared Studies of Carbon Monoxide Hydrogenation Over Alumina-Supported Ruthenium

ABSTRACT

The nature of the species present on a Ru/Al_2O_3 catalyst during CO hydrogenation was studied by means of Fourier transform infrared spectroscopy. Three forms of adsorbed CO were identified, designated as linearly-adsorbed, diadsorbed, and μ-bridge adsorbed. The coverage by the linearly-adsorbed form of CO obey a Langmuir isotherm under reaction conditions. The equilibrium constant associated with this isotherm is given by $K_{CO} = 1.1 \times 10^{-9} \exp(25{,}000/RT)\ atm^{-1}$. The diadsorbed species is associated with individual Ru atoms and clusters and, in contrast to linearly-adsorbed CO, does not readily undergo hydrogenation at temperatures below 548K. The μ-bridge form of adsorbed CO may involve either a pair of Ru sites or a Ru site and an adjacent Lewis acid site. Hydrocarbon, formate, and carbonate structures were also observed in the course of this study. It was established, however, that these species are present on the alumina support and are not intermediates of CO hydrogenation over Ru.

INTRODUCTION

Infrared spectra taken during the hydrogenation of CO over ruthenium catalysts have helped to identify the dominant species adsorbed on the catalyst (1-5). Dalla Betta and Shelef (1) have reported that the surface of a Ru/Al_2O_3 catalyst is nearly saturated by adsorbed CO at temperatures up to 523K. It was suggested that the presence of hydrogen on the catalyst surface weakens the C-O bond of chemisorbed CO, since the band for this species appeared at a lower frequency than that observed for CO chemisorbed in the absence of hydrogen. At higher temperatures the build up of carbon on the catalyst caused a further shift of the CO bond to lower frequencies and a decrease in the band intensity. Bands attributable to hydrocarbon, formate, and carbonate structures were also observed but these species were ascribed to reaction products adsorbed on the support. Chemisorbed CO has also been observed as a dominant species in the studies conducted by Ekerdt and Bell (2,3) using a Ru/SiO_2 catalyst. In this work the position and intensity of the CO band were found to be independent of the H_2/CO ratio or the CO partial pressure. A decrease in the band intensity, unaccompanied by a shift in position, was observed with increasing temperature and was ascribed to a reduction in the CO coverage. Bands were also observed for hydrocarbon species. These structures could be removed from the catalyst surface by hydrogenation, but did not appear to be intermediates in the synthesis of stable products. Additional observations concerning the hydrocarbon structures formed on Ru/SiO_2 and Ru/Al_2O_3 catalysts have been presented by King (4,5). Strong bands attributable to long-chain saturated hydrocarbons were observed at temperatures below

473K. While the exact point of attachment of these structures could not be defined, it was concluded that the species observed were not intermediates in the formation of gas phase products. At higher temperatures, changes in the shape and position of the hydrocarbon band suggested the presence of short-chain species. It was proposed that these species are attached to the metal surface and might be intermediates in the synthesis reaction.

The primary objective of the present investigation was to characterize more fully the influence of reaction and concentration of the species adsorbed on a Ru/Al_2O_3 catalyst during CO hydrogenation. Fourier transform infrared spectroscopy was used for this purpose, and particular attention was devoted to interpretation of the bands ascribed to chemisorbed CO. Working under conditions chosen to avoid significant catalyst deactivation, three different forms of adsorbed CO were identified. These are designated as linearly-adsorbed, diadsorbed, and μ-bridge adsorbed CO. A detailed study was made of the effects of reaction conditions on the position and intensity of the band associated with the linearly-adsorbed CO. Based on these observations, estimates were made of the variation in the coverage by this species with CO partial pressure and catalyst temperature. As a complement to these studies the kinetics of forming C_1 through C_{10} hydrocarbons were examined in detail. The results of these efforts together with a discussion of the mechanism of hydrocarbon synthesis over ruthenium will be presented separately (6).

EXPERIMENTAL

The 1% Ru/Al_2O_3 catalyst used for these studies was prepared by adsorption of the $Ru_6C(CO)_{17}$ from pentane solution onto Kaiser KA-201 alumina. Details concerning synthesis of the complex, impregnation of the support and the reduction of the final catalyst are described in references (6,7). A 75 mg portion of the reduced catalyst was pressed into a 20 mm by 0.25 mm disk and placed inside a small infrared reactor (8).

Prior to each series of experiments, the catalyst was reduced in flowing H_2 for 10 to 12 hours at 673K and 10 atm. The temperature was then lowered to 498K and a premixed feed, containing H_2 and CO, was introduced at a flow rate of 200 cm^3/min (NTP). Ten minutes after reaction had begun, the effluent gas was analyzed by gas chromatography (6), and the gas feed was switched over to pure H_2 for 1 hour. By alternating short reaction periods and longer reduction periods, a stable catalyst activity could be achieved after several cycles. This procedure also eliminated the build up of large amounts of carbon and the concurrent deactivation of the catalyst. Once a stable catalyst activity had been obtained, reaction conditions were adjusted to those desired for a particular experiment.

Infrared spectra were taken with a Digilab FTS-10M Fourier transform infrared spectrometer, using a resolution of 4 cm^{-1}. For the observation of steady state phenomena, 100 interferograms, each acquired in about 1.25 s, were co-added to improve the signal to noise ratio. However, good spectra could also be obtained by co-adding as few as 10 interferograms. In addition to recording spectra of the catalyst under reaction conditions, spectra were also recorded of the catalyst, following reduction in H_2, and of a support disk, placed downstreak from a catalyst disk, during reaction. The latter two spectra were used to subtract out infrared adsorptions due to the support and the gas phase.

RESULTS AND DISCUSSION

Infrared spectra of the catalyst taken under reaction conditions showed bands in two regions, one set appearing between 3200 and 2400 cm^{-1} and another set appearing between 2300 and 1200 cm^{-1}. The bands in the first of these regions are associated with adsorbed hydrocarbons, while bands in the second region are due to carbonyl, carbonate, and formate structures. To identify whether these structures are present on the surface of the metal and/or support and to identify the relative stability and reactivity of individual structures, spectra were taken under a variety of conditions.

Bands Observed Between 2300 and 1200 cm^{-1}

Spectral Observations - Representative spectra of the most prominant features observed in this region, during reaction at pressures of 1, 5, and 10 atm, are shown in Fig. 1a. The spectrum shown at each pressure represent the difference in the adsorbances of the catalyst and reference disks, measured in the presence of the same gas composition. A broad band can be seen near 2000 cm^{-1} superimposed on which is a weakly defined shoulder of 2040 cm^{-1} and a partially resolved band at 1960 cm^{-1}. All three features appear immediately upon passage of the H_2-CO mixture over the catalyst and the integrated intensity of the band envelope grows by about 10-15% over a 20 minute period of

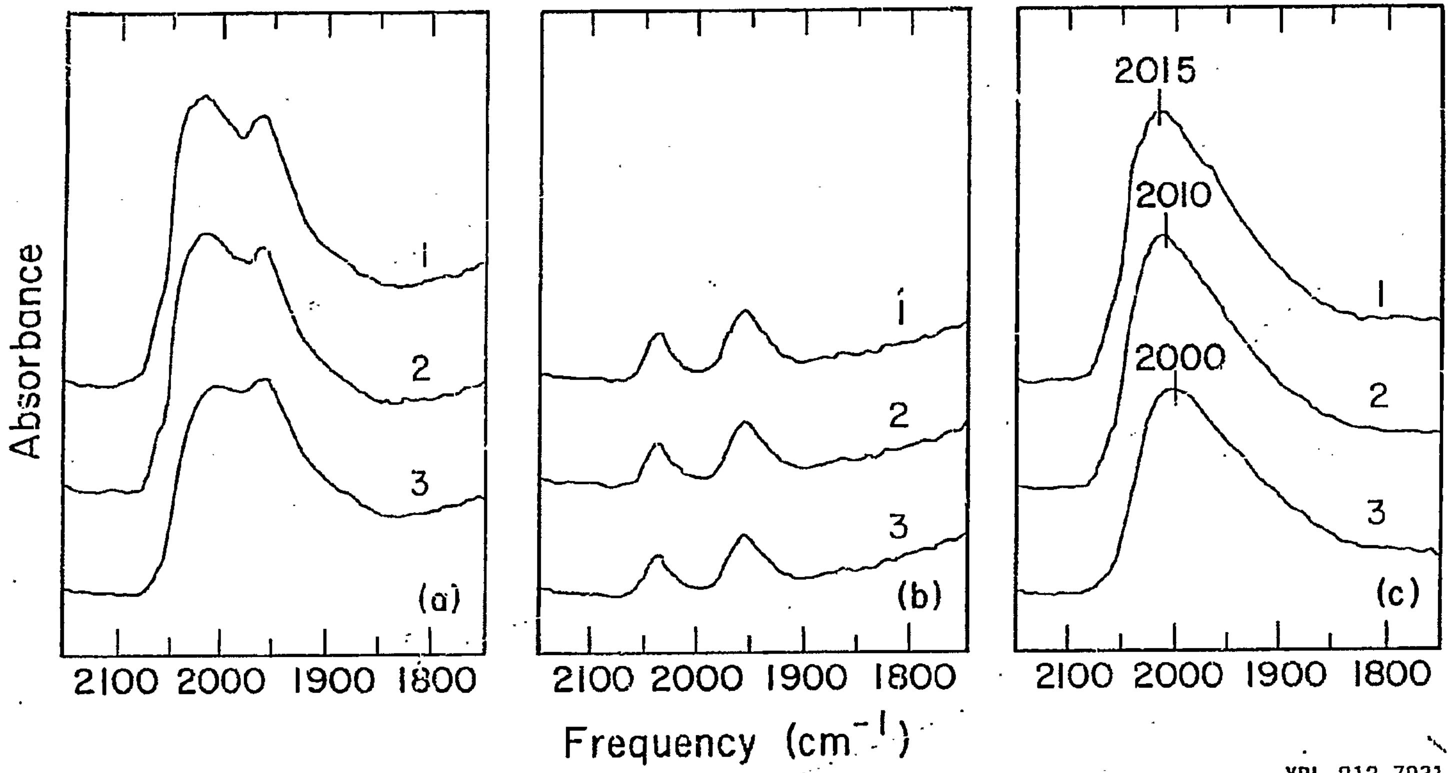

XBL 812-7931

Fig. 1. Spectra obtained at 548K during reaction and subsequent reduction in H_2: (a1) P = 10 atm, $H_2/CO = 2$; (a2) P = 5 atm, $H_2/CO = 2$; (a3) P = 1 atm, $H_2/CO = 2$; (b1) after (a1) and following reduction in H_2 at 10 atm; (b2) after (a2) and following reduction in H_2 at 5 atm; (b3) after (a3) and following reduction in H_2 at 1 atm; (c1) difference between (a1) and (b1); (c2) difference between (a2) and (b2); (c3) difference between (a3) and (b3).

observation. It is significant to note, though, that the positions of the three bands are totally unaltered during this period. Figure 1b shows spectra taken following cessation of the reaction and reduction in H_2. The intense band near 2000 cm^{-1} is now completely eliminated, thereby revealing very clearly the bands at 2040 and 1960 cm^{-1}. It is noted that the intensities of these two peaks are independent of the reaction pressure. Moreover, the structures giving rise to these features are stable to reduction at temperatures below 548K and can only be removed at higher temperatures. Spectra of the species removed by reduction at reaction temperatures are shown in Fig. 1c, and are obtained by taking the difference between the spectra presented in Figs. 1a and 1b. Each spectrum consists of a broad, asymmetric band which does not return to the baseline at low frequencies. With increasing reaction pressure, the intensity of this band increases and the band maximum shifts to higher frequencies.

The effects of temperature on the spectra of the species susceptible to H_2 reduction are illustrated in Fig. 2. The spectra shown in this figure represent the difference between spectra taken under reaction conditions and those obtained following H_2 reduction of the catalyst at the reaction temperature. This mode of presentation is similar to that used in Fig. 1c, with the exception that bands associated with the gas phase and species weakly bound to the support are not subtracted out. The series of peaks occurring between 2300 cm^{-1} and 2060 cm^{-1} is due to gas phase CO. These bands are clearly evident in spectrum e, which was obtained at the conditions of spectrum b using a disk of alumina free of Ru. Both the position and intensity of the

Fig. 2 Spectra of chemisorbed CO under reaction conditions and following adsorption of CO: (a) sample spectrum - $H_2/CO = 2$, $P = 1$ atm, $T = 498K$; reference spectrum - after reduction in H_2 at 1 atm and 498K; (b) sample spectrum - $H_2/CO = 2$, $P = 1$ atm, $T = 523K$; reference spectrum - after reduction in H_2 at 1 atm and 523K; (c) sample spectrum - $H_2/CO = 2$, $P = 1$ atm, $T = 548K$; reference spectrum - after reduction in H_2 at 1 atm and 548K; (d) sample spectrum - after CO adsorption at 1 atm and 523K and elution of gas phase CO with He; reference spectrum - after reduction in H_2 at 1 atm and 523K; (e) sample spectrum - $H_2/CO = 2$, $P = 1$ atm, $T = 523K$; reference spectrum - after reduction in H_2 at 1 atm and 523K.

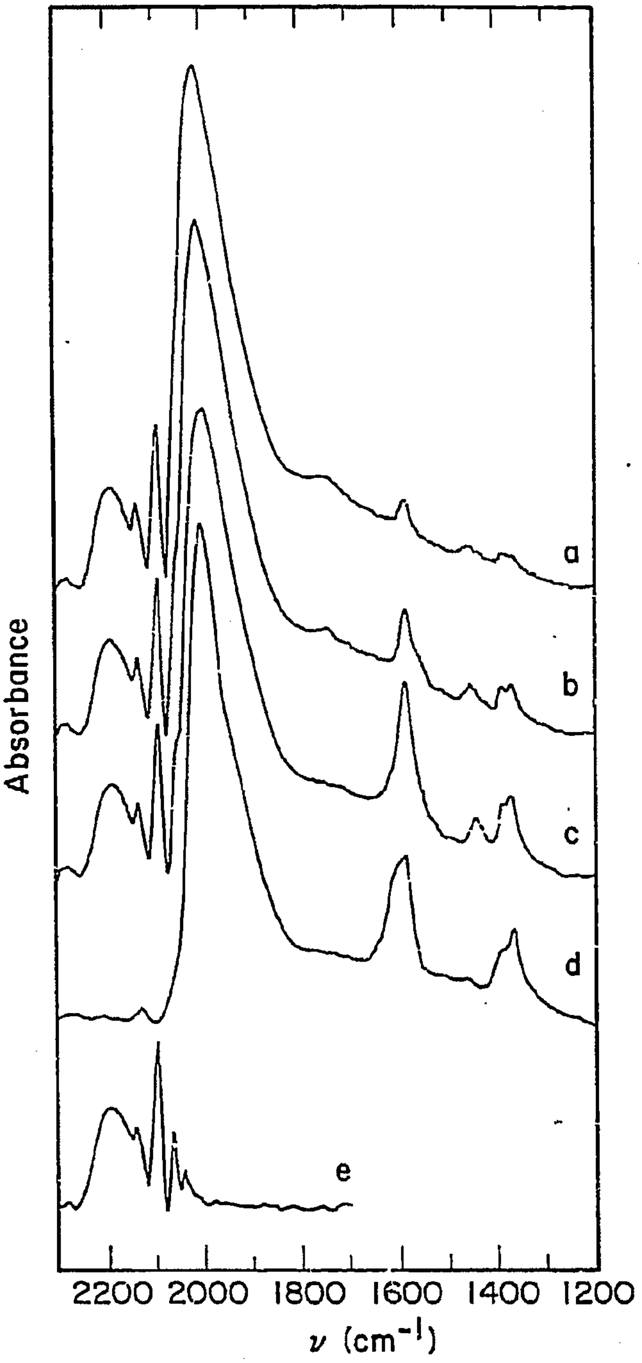

XBL 812-7930

Fig. 2.

band near 2000 cm^{-1} depend on the catalyst temperature. As the temperature increases, the band maximum shifts to lower frequencies and the intensity decreases.

In addition to the major features appearing at 2000 cm^{-1}, a broad band can be seen in Fig. 2, which extends between 1800 and 1200 cm^{-1}. Superimposed on this band are five more sharply defined bands at 1750, 1590, 1450, 1390, and 1370 cm^{-1}. Only the weak band at 1750 cm^{-1} is due to chemisorbed CO. Based upon the studies of Dalla Betta and Shelef (1) and King (4,5), the bands at 1590, 1390, and 1370 can be assigned to formate structures, and the band at 1450 cm^{-1} can be assigned to carbonate structures. Both types of species are formed on the alumina support and accumulate during reaction. Upon reduction of the catalyst in H_2, the intensity of the bands associated with these spectra diminish. As a result, the background spectra used in obtaining the spectra presented in Fig. 2 show a decrease in the intensity of the formate and carbonate bands with increasing temperature, and, consequently these bands are emphasized in the difference spectra shown.

The similarity of spectra obtained under reaction conditions with those obtained by exposure of the catalyst to CO alone can be seen by comparison of spectra b and d in Fig. 2. The latter spectrum was obtained after passing CO over the catalyst for 5 min and then eluting the gaseous CO with He for 0.5 min. With the exception of the gas phase bands, which are not present in spectrum d, spectra b and d are virtually identical.

A more detailed illustration of features appearing on the low frequency side of the principle carbonyl band is shown in Fig. 3. This spectrum is similar to spectrum d in Fig. 2 but was obtained at 448K. At this temperature the formate and carbonate structures are not removed upon reduction and consequently the bands associated with these species are subtracted out completely. The broad band between 1800 and 1200 cm^{-1} is now seen to be composed of two broad bands centered at approximately 1700 and 1500 cm^{-1}. In addition, a definite shoulder can be observed at 1920 cm^{-1}, on the low frequency side of the band near 2000 cm^{-1}.

All of the bands observed in Figs. 1 and 2 are attenuated slowly upon passage of He over the catalyst and much more rapidly in the presence of H_2. An illustration of these changes is shown in Fig. 4. Passage of He over the catalyst causes a slow decrease in the intensity of the principle band and a concurrent downscale shift in its position. More careful examination of spectra 1 through 4 reveals that initially intensity is lost from the high frequency portion of the principle adsorption band and from the peaks present below 1900 cm^{-1}. This observation is supported by spectrum 1 in Fig. 4c, which represents the difference between spectra 1 and 2 in Fig. 4a. With increasing time, the region from which intensity is lost shifts towards lower frequencies, indicating that the position of the high frequency component of the principle band shifts to lower frequencies as its intensity decreases. Eventually, though, intensity is lost from both the high and low frequency regions of the principle adsorption band and from the peak located near 1700 cm^{-1}. Spectra 2, 3, and 4 in Fig. 4c illustrates these changes.

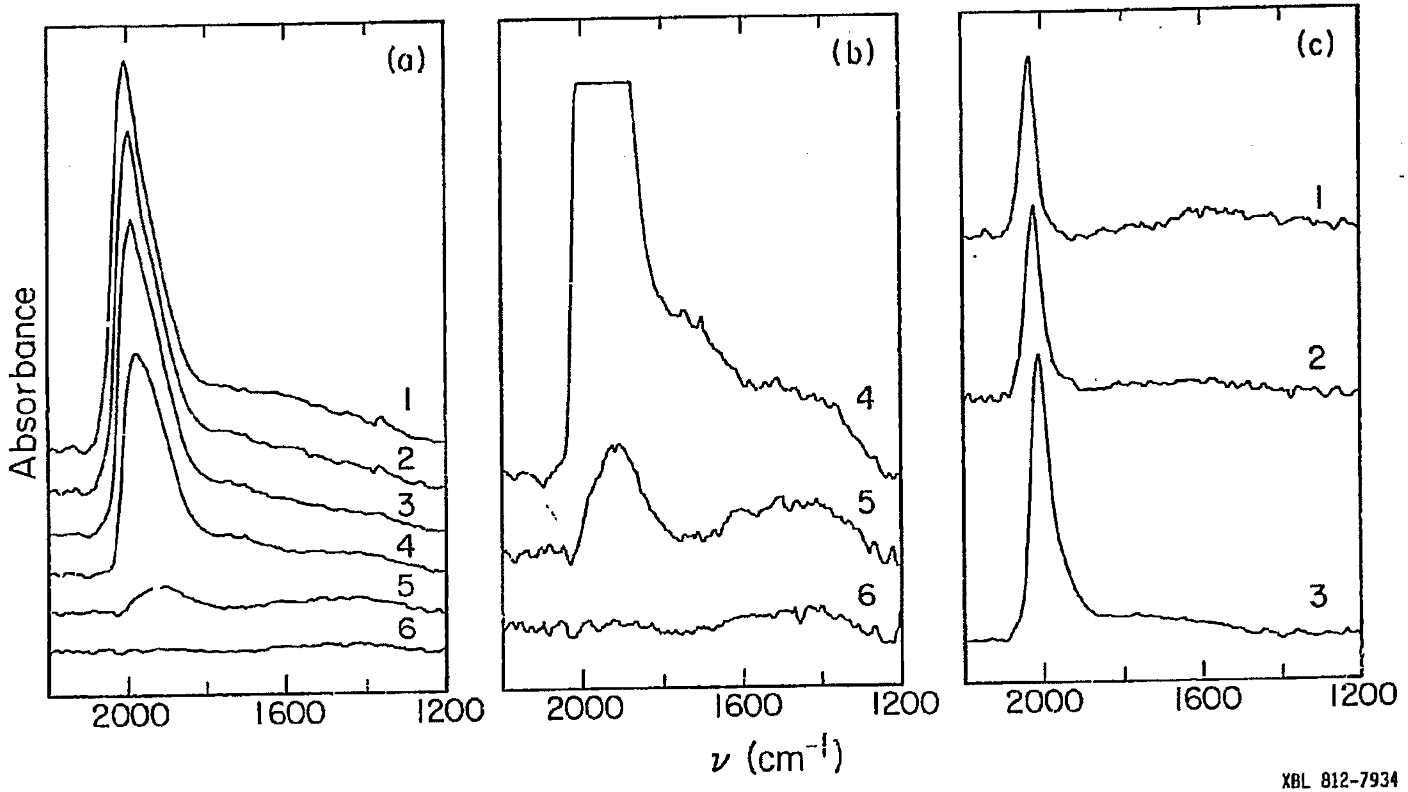

XBL 812-7934

Fig. 4. Effects of He and H_2 on the intensities of bands associated with adsorbed CO: adsorption conditions - P_{CO} = 3.3 atm, T = 498K; (a1) following exposure to a He flow at 498K for 0.5 min; (a2) 2.7 min; (a3) 14.0 min; (a4) 46.0 min; (a5) following exposure to a H_2 flow at 498K for 0.2 min; (a6) 0.5 min; (b4) same as (a4) expanded fourfold; (b5) same as (a5) expanded fourfold; (b6) same as (a6) expanded fourfold; (c1) difference between (a1) and (a2) expanded twofold; (c2) difference between (a2) and (a3) expanded twofold; (c3) difference between (a3) and (a4) expanded twofold.

The relationship between the position of the principle band and the relative integrated adsorbance of the band is shown in Fig. 5. If it is assumed that the extinction coefficient associated with this band is constant, then the abscissa in this figure is equivalent to a fractional surface coverage. The plot is seen to consist of two distinct branches. As the ratio A/A_s decreases from unity, ν_{CO} shifts from 2030 cm^{-1} to lower values but at an ever decreasing rate. When A/A_s reaches 0.55, the decrease in $_{CO}$ accelerates. Finally, at $A/A_s = 0.2$, ν_{CO} reaches a value of 1950 cm^{-1}.

Figure 4 also shows that the reduction of preadsorbed CO in H_2 causes a very rapid decline in the intensity of the high frequency side of the principle band and of the broad band centered at 1700 cm^{-1}. As a consequence, the bands located at 1920 cm^{-1} and 1500 cm^{-1} can now be seen more clearly. Spectrum 3 in Fig. 4b shows that the bands are also attenuated as the duration of reduction is extended.

Assignment of Carbonyl Bands - The present results show that as many as six bands can be identified for chemisorbed CO, located at 2040, 2030-1950, 1920, 1750, 1700, and 1500 cm^{-1}. The assignment of these features to specific structures is examined next, following which the stability and reactivity of the various forms of adsorbed CO are discussed.

The strong band observed between 2030 and 1950 cm^{-1} falls within the range of frequencies (2085 to 1950 cm^{-1}) associated with linearly-bonded CO in Ru carbonyl complexes (9). As a result, it is reasonable to assign this band to linearly-adsorbed CO. This interpretation is further supported by recent EELS (10) and reflectance infrared (11)

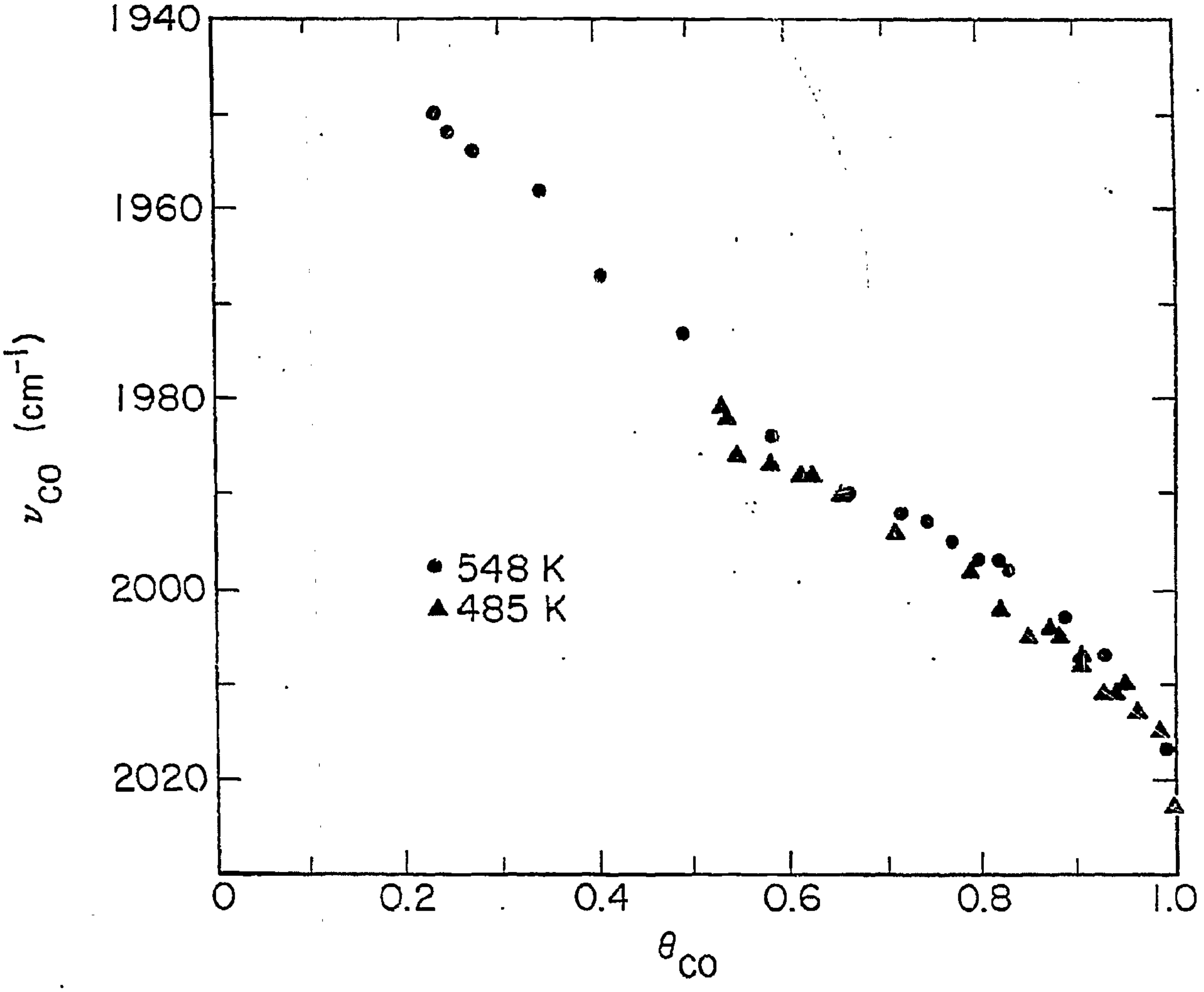

XBL 812-7924

Fig. 5. Relationship between the frequency of the principle carbonyl adsorption band and the coverage by linearly adsorbed CO.

studies of CO adsorbed on a Ru (001) surface. The spectra obtained in these investigations exhibit a single band which shifts with increasing CO coverage from about 1980 cm^{-1} to as high as 2080 cm^{-1}, as a result of strong lateral interactions in the adlayer. LEED (10, 12-14) and ESDIAD (15) observations support the assignment of this band to linearly-adsorbed CO.

While the shift in band position with coverage, observed in the present work is of the same magnitude as that reported for CO adsorption on Ru (001) surfaces (10,11), the highest and lowest frequencies observed in the single crystal studies are notably higher than those shown in Fig. 5. This difference may be due to differences between the physical properties of alumina-supported Ru microcrystallites and bulk Ru metal. It is also possible that at least a part of the difference may be due to the presence of carbon on the surface of the supported Ru, formed by CO disproportionation. Carbon has been found to act as an electron donor and to enhance the back-donation of electronic charge from the metal to the π^* orbitals of CO (1). This would have the effect of weakening the C-O bond and shifting its frequency downscale. It is significant to note, that while carbon deposition via CO disproportionation has been observed for alumina-supported Ru (16, 17), no evidence has been reported for the occurrence of this reaction on Ru (100), (001), (1010), (110) surfaces studied at low pressures (12,18-21).

As was noted earlier, during reaction the band near 2000 cm^{-1} undergoes a moderate (10-15%) growth in intensity which is unaccompanied by changes in the band position. A plausible explanation for this observation is that the Ru dispersion increases slightly with time of reaction but that the fractional coverage of the surface remains the same. The fact that such changes are not observed upon exposure of the catalyst to CO alone and that the rate of change is accelerated by higher reaction pressure, at a fixed H_2/CO ratio and temperature, suggests that the changes in Ru dispersion may be caused by the local release of the heat of CO hydrogenation. Under this influence some of the smaller three-dimensional microcrystallites may be converted to two-dimensional rafts, thereby exposing a greater fraction of surface Ru atoms.

The spectra presented in Figs. 1 and 2 indicate that both the frequency and intensity of the band assigned to linearly-adsorbed CO decrease with decreasing CO partial pressure and catalyst temperature. Since, as was shown in Fig. 3, the spectra observed for CO chemisorbed in the presence and absence of H_2 are virtually identical, it seems reasonable to propose that the changes observed under reaction conditions can be ascribed to changes in the coverage of the Ru surface by linearly-adsorbed CO. Because of the increase in band intensity with duration of reaction, discussed above, band intensity cannot be used as a reliable measure of the coverage of linearly-bonded CO. An estimate of the fraction of the total sites which could be covered at saturation by this species can be attained, however, by assuming that the extinction coefficient for the band near 2000 cm^{-1} is independent of coverage and then using the relationship between frequency and coverage noted in Fig. 5. It should be noted, though, that the assumption underlying such calculations is not fully established. In studies conducted by Pfnur et. al. (11), the intensity of the infrared band associated with CO chemisorbed on a Ru (001) surface was found to increase linearly with CO coverages, up to a coverage of one half of saturation. For higher coverages, the integrated intensity declined. These results would suggest that the extinction coefficient decreases at coverages approaching saturation. However, since only a monotonic change in integrated intensity with coverage was observed in the present work, it can be concluded that the trend observed for a Ru (001) surface does not necessarily apply to alumina-supported Ru microcrystallites.

Applying the approach described above, a series of isotherms can be constructed to determine the coverage of linearly-adsorbed CO under reaction conditions. Figure 6 shows that on a plot of θ_{CO}^{-1} versus P_{CO}^{-1} the data fall along straight lines, independent of the H_2 partial pressure. Consequently θ_{CO} can be described by a Langmuir isotherm of the form

$$\theta_{CO} = \frac{K_{CO}P_{CO}}{1 + K_{CO}P_{CO}} , \qquad (1)$$

where K_{CO} is the effective equilibrium constant for CO adsorption. From the slopes of the lines presented in Fig. 6 it is determined that

$$K_{CO} = 1.1 \times 10^{-9} \exp(25{,}500/RT)\text{atm}^{-1} \qquad (2)$$

The heat of adsorption appearing in eqn. 2 is in excellent agreement with activation energies for CO desorption determined in studies conducted with alumina-supported Ru (17) and Ru single crystals (18-22).

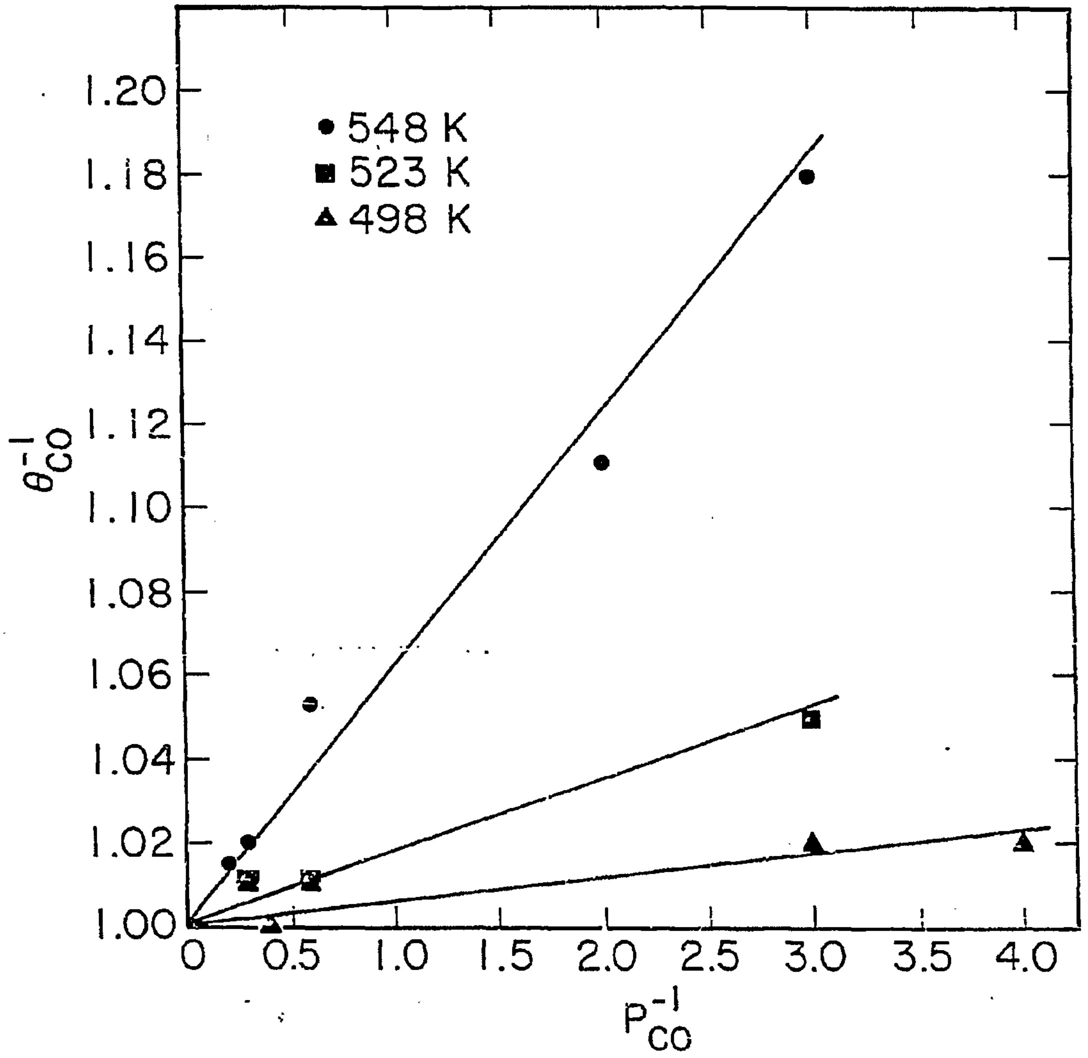

XBL 812-7925

Fig. 6. Relationship between θ_{CO}^{-1} and P_{CO}^{-1} during reaction.

The preexponential factor, though, is two orders of magnitude smaller than that calculated from data presented by Pfnür et al. (22) for CO desorption from a Ru (001) surface at high CO coverages. A possible explanation for this difference may be that the frequency factor for CO desorption from the surface of alumina-supported Ru is two orders of magnitude higher than that for desorption from a Ru (001) surface.

The observations concerning the band for linearly-adsorbed CO reported here are in qualitative agreement with previous studies of a similar nature, but some differences exist with regard to the interpretation of the shifts in band position with reaction conditions. Working with a 5% Ru/Al_2O_3 catalyst, Dalla Betta and Shelef (1) reported that the spectrum of CO adsorbed at 523K from a 1 atm CO/He mixture (0.025:0.975 mole fraction) exhibited a single band centered at 2043 cm^{-1}. When the catalyst was contacted with an H_2/CO/He mixture (0.075:0.025:0.900) at the same temperature and pressure, the band shifted to 1996 cm^{-1}, and the integrated band intensity decreased by 12%. A similar effect of H_2 was noted by King (4) in studies performed with a 1% Ru/Al_2O_3 catalyst. Dosing the catalyst with CO at room temperature produced a band at 2045 cm^{-1} which shifted to 2020 cm^{-1} following exposure of the adsorbed CO to an H_2 pressure of 5.4 atm. Both Dalla Betta and Shelef (1) and King (4) have proposed that the shift in CO frequency could be attributed to an increase in the availability of electrons for back-bonding from the metal to the adsorbed CO, resulting from the presence of coadsorbed H atoms. While this interpretation is plausible, it seems that one could equally well explain these observations in terms of a decrease in the dipole-dipole interactions resulting from a small change in the surface coverage by CO (11). As may be seen in Fig. 5, a 15% decrease in the integrated absorbance of the band from its maximum value corresponds to a shift in the band from 2030 cm^{-1} to 2000 cm^{-1}.

Dalla Betta and Shelef (1) and King (4) reported that increasing the temperature while passing a continuous flow of H_2 and CO over the catalyst caused a downscale shift in the position of the band for linearly-adsorbed CO and a reduction in the band intensity. Provided temperatures did not exceed ~523K and reaction times were relatively short, the initial CO band could be restored simply by cooling the catalyst in the following H_2/CO mixture. At higher temperatures and with durations of reaction exceeding several hours, much of the CO band intensity remained lost upon cooling. Dalla Betta and Shelef (1) associated the irreversible charges in CO band position and intensity to the interaction of the metal with a carbonaceous deposit. King (4) concurs with this explanation but suggests that the reversible changes in the band characteristics are due to depletion via reaction of more weakly bound forms of CO which exhibit adsorptions towards the high frequency side of the CO band.

In the present study the duration of reaction was kept to less than 20 min and the temperature never exceeded 548K, in order to avoid extensive catalyst deactivation due to the build up of carbon. As a result, it is believed that the changes in CO band frequency and intensity with temperature shown in Fig. 2 are not due to the accumulation of carbon on the catalyst surface but, rather, to changes in the coverage of linearly-adsorbed CO.

The bands observed at 2040 and 1960 cm^{-1} in the present work are very similar to those reported by Kuznetsov et al. (7) in their studies of the structures formed upon decomposition of alumina-supported $Ru_3(CO)_{12}$, α-$H_4Ru_4(CO)_{12}$, and $Ru_6C(CO)_{17}$. In each case, reduction of the supported cluster in H_2 at temperatures less than 573K led to the appearance of two bands of nearly comparable intensity, located at 2047-2052 and 1955-1970 cm^{-1}. Comparison of the positions of these bands with those for Ru-halocarbonyl complexes leads to the conclusion that the two bands arise from structures of the form $[Ru(CO)_2X_2]_n$ (7,9). The element X in this structure is assumed to be the oxygen of the alumina lattice and the number n represents the number of Ru atoms present in the surface structure.

Consistent with the proposed interpretation, the bands appearing at 2040 and 1960 cm^{-1} can be associated with the symmetric and asymmetric modes of vibration of C-O bonds in a pair of CO molecules attached to a common Ru site. The angle between the two CO molecules, 2α, can be estimated from the ratio of the integrated adsorbances of the symmetric and asymmetric bands, A_{sym} and A_{asym}, by means of eqn. 3 (23-25).

$$A_{asym}/A_{sym} = \tan^2\alpha \tag{3}$$

This relationship has been shown to provide an accurate measure of α for dicarbonyl transition metal complexes in which the two CO ligands are in a cis configuration. Application of eqn. 3 to the bands at 1960 and 2040 cm^{-1} leads to an estimate of $100^\circ \pm 5^\circ$ for the angle between the two CO molecules attached to a common Ru site. By way of comparison, it is noted that bond angles between 93 and 96° have been reported for $(\pi\text{-}C_5H_5)Fe(CO)_2X$ (X = Cl, Br, I) and a bond angle of 91° has been reported for $Rh_2(CO)_4Cl_2$ (24,26). Thus, it appears that the angle between diadsorbed CO molecules is similar to that found for transition metal complexes.

The independence of the vibrational frequencies associated with the diadsorbed CO structures on the coverage by singly-adsorbed CO indicates that the two structures are, most likely, not coupled by dipole-dipole interactions (25). This observation, together with the fact that the diadsorbed CO is much more stable to decomposition or reduction than monoadsorbed CO, suggest that the diadsorbed structures occur at sites isolated from the Ru crystallites. Examples of such sites might be individual Ru atoms or small Ru clusters. This interpretation is supported by the fact that the intensity of the bands at 2040 and 1960 cm^{-1} can be attenuated significantly by extended exposure of the catalyst to CO without affecting the intensites or positions of other CO bands (27).

The band appearing at 1920 cm^{-1} in Fig. 5b occurs at a frequency about 30 cm^{-1} lower than that normally ascribed to linearly-bonded CO in unsubstituted Ru carbonyls. However, C-O vibrational frequencies as low as 1900 cm^{-1} have been observed for linearly-bonded CO in Ru carbonyl complexes containing nucleophilic ligands (9). In view of this, the band at 1920 cm^{-1} can be assigned to CO adsorbed in a linear mode at a site adjacent to a nucleophilic adsorbate. The most likely candidate for the latter species is carbon, formed as an intermediate in either CO disproportionation or hydrogenation.

The weak peak at 1750 cm^{-1} and the broad peaks at 1700 and 1500 cm^{-1} appear at frequencies much lower than those normally associated with bridging carbonyls (1880-1813 cm^{-1}) in Ru complexes (9). Recent studies have shown that CO vibrations do occur in this portion of the spectrum for μ-bonded carbonyls, in which coordination occurs through both the carbon and oxygen atoms of CO, and for adducts formed between metal carbonyls and Lewis acids. When coordination takes place exclusively with metal atoms, CO frequencies of 1645 cm^{-1} for $Mn_2(CO)_5(Ph_2PCH_2PPh_2)_2$ (28) and 1330 cm^{-1} for $(\eta^5\text{-}C_5H_5)_3Nb_3(CO)_7$ (29) have been observed. The large difference in these frequencies reflects the fact that μ-bonding can occur in different ways. In the case of adducts of metal carbonyls with Lewis acids, C-O stretching frequencies are observed in the range of 1530-1700 cm^{-1} (9,30). In the case of $Ru_3(CO)_{12}\cdot AlBr_3$, a strong band is seen at 1535 cm^{-1} and spectra of the 1:1 and 1:2 adducts of $[(\pi\text{-}C_5H_5)Ru(CO)_2]_2$ with isobutyl aluminum exhibit a band at 1680 cm^{-1} (9,30).

Reactivity of Carbonyl Structures - The spectra presented in Figs. 1 and 3 demonstrate that the different forms of adsorbed CO exhibit significant differences in reactivity with respect to H_2. The two types of linearly-adsorbed CO, which are characterized by the band appearing between 2030 and 1950 cm^{-1} and the band appearing at 1920 cm^{-1}, react rapidly with H_2. Transient response experiments (31) have shown that the dynamics of the disappearance of these bands correlate closely with the formation of methane and water, which suggests that linearly-adsorbed CO is the primary source of carbon for the synthesis reaction. Figure 3 shows that the band at 1700 cm^{-1} is also attenuated rapidly during H_2 reduction. No study has been made of the reaction dynamics associated with this band and hence it is not possible to conclude whether the μ-bonded form of CO which this band represents is an important reaction precursor.

The pair of bands at 2040 and 1960 cm^{-1} are relatively stable to reduction and attenuate only slowly at temperatures below 546K. This fact, plus the general behavior of these bands, suggests that diadsorbed CO does not enter into the synthesis of hydrocarbons under the reaction conditions examined in these studies. Consistent with this conclusion, it has been found (27) that catalysts which exhibit a high proportion of diadsorbed CO relative to singly adsorbed CO are less active than catalysts which exhibit the reverse relationship between the two forms of adsorbed CO. The μ-bonded form of CO characterized by the band at 1500 cm^{-1} is only slightly less reactive than the linearly-adsorbed form of CO. However, because of the weak intensity of this band it has not been possible to relate the intensity of this band to the catalyst activity.

Bands Observed Between 3200 and 2400 cm^{-1}

Figure 7 shows a sequence of spectra for the frequency range between 3200 and 2400 cm^{-1}, taken at different times during the course of a run. The spectrum taken after 0.5 min shows only a very noisy baseline due to the poor transmission of the catalyst disk in this frequency regime. After 10 min of reaction, well defined peaks can be detected at 2930 and 2860 cm^{-1}. The intensity of these features increase steadily with time and after 20 min a shoulder can be detected at 2960 cm^{-1} in addition to the two more intense bands. It is signifi-

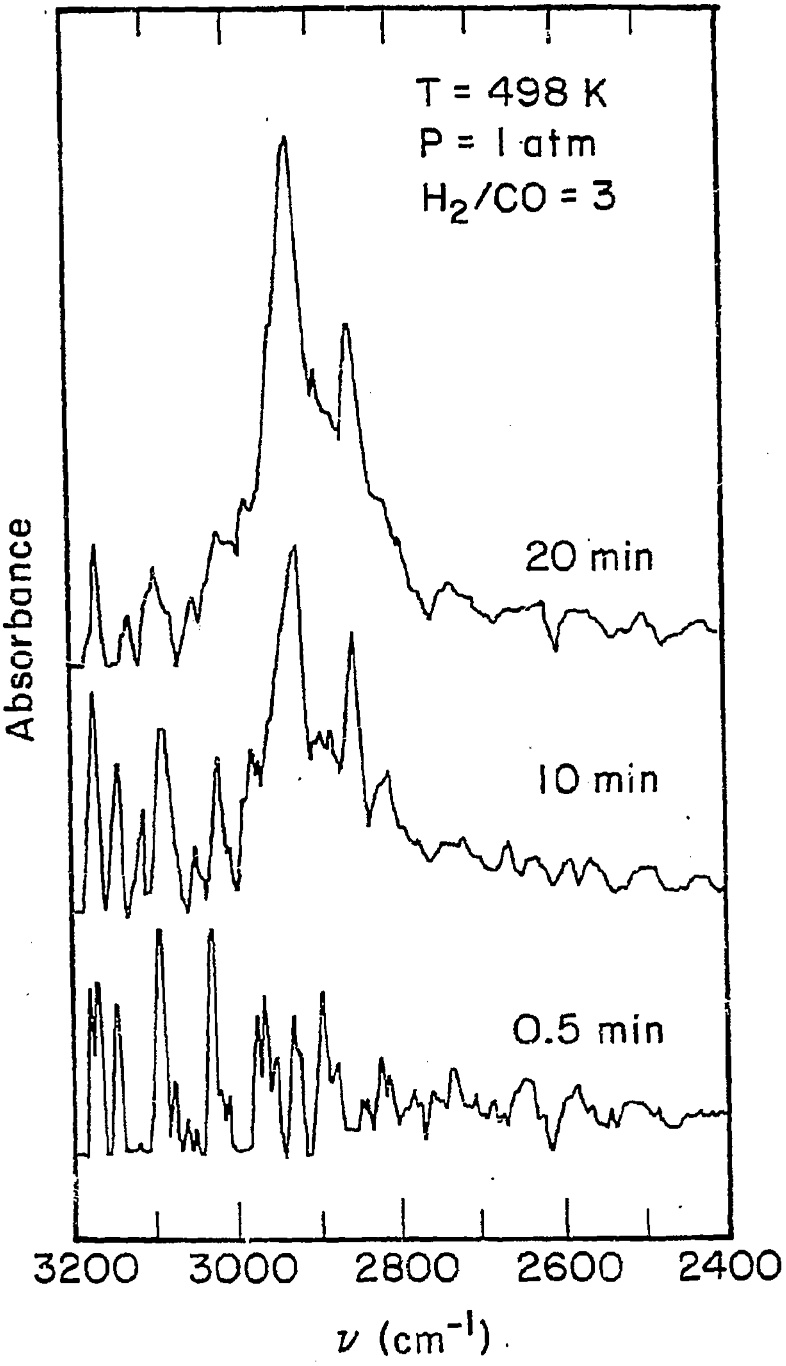

XBL 812-7909

Fig. 7. Effects of reaction duration on the intensities of bands appearing between 2400 and 3200 cm^{-1}: H_2/CO = 3; P = 1 atm; T = 498K.

cant to note that over the same period of time the intensity of the principle CO band increases by less than 8% and its position remains fixed at 2010 cm^{-1}.

Spectra of the C-H stretching region taken at different temperatures, pressures, and H_2/CO ratios exhibit the same set of bands observed in Fig. 7. By way of illustration, three spectra are shown in Fig. 8, taken after 10 min of reaction at temperatures of 498, 523, and 548K; a pressure of 10 atm; and an H_2/CO ratio of 2. It is seen that the positions of the three bands remain fixed and are insensitive to changes in the reaction conditions. The increase in band intensities with increasing temperature can be associated with the more rapid rate of accumulation of species adsorbing infrared radiation in this portion of the spectrum.

The stability of the bands seen in Figs. 7 and 8 were examined by treating the catalyst in various gas mixtures following reaction. Purging the reactor with He or a CO/He mixture at reaction temperature had no effect on the band intensities. The bands were rapidly attenuated, though, when a H_2/He mixture was introduced into the reactor. The rate of attenuation was found to increase with increasing catalyst temperature and H_2 partial pressure.

Efforts were also made to determine whether the features appearing in Figs. 7 and 8 might be associated with reactions occurring on the alumina support. Passage of H_2/CO mixtures over an alumina disk failed to produce any bands over the temperature interval of 498 to 548K. Weak bands were observed, though, when an alumina disk was placed in a cell immediately downstream of the cell containing the catalyst disk.

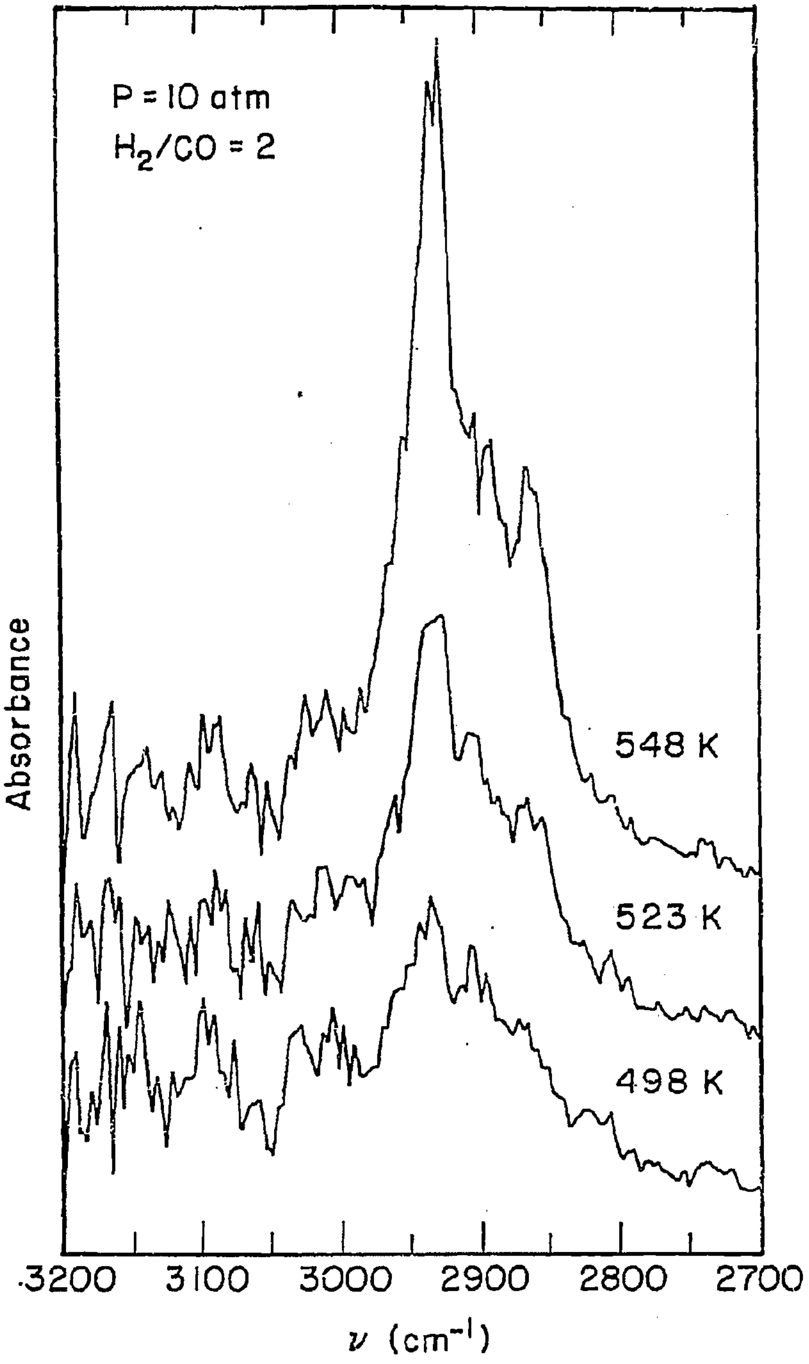

XBL 812-7910

Fig. 8. Effects of temperature on the intensities of bands appearing between 2400 and 3200 cm^{-1}: H_2/CO = 2; P = 10 atm; observation time = 10 min.

Since the positions of the bands were identical to those observed in Figs. 7 and 8, these bands most likely arise from the adsorption of hydrocarbon products on the alumina disk.

The positions of the three bands found here are virtually identical to those which have been reported by Dalla Betta and Shelef (1), Ekerdt and Bell (2,3), and King (4,5) in studies of CO hydrogenation over alumina- and silica-supported Ru catalysts. The bands at 2930 and 2861 cm^{-1} can be assigned to the asymmetric and symmetric stretching of CH_2 groups present in saturated compounds, and the shoulder at 2960 cm^{-1} can be assigned to a methyl group (9). It is significant to note that in contrast to the work carried out by King (4,5) with a Ru/Al_2O_3 catalyst, the position of the bands did not shift upscale with increasing reaction temperature and no hydrocarbon structures were formed by the interaction of CO and H_2 over alumina devoid of Ru.

Based on infrared spectra taken during CO hydrogenation over a Ru/Al_2O_3 catalyst, Dalla Betta and Shelef (1) concluded that the hydrocarbon bands observed could be ascribed to reaction products accumulated on the alumina support. The results of the present study also agree with this interpretation. The monotonic growth of the hydrocarbon bands beyond the point at which steady state reaction has been attained, and the absence of any influence of the hydrocarbon band growth on the position or intensity of the CO band indicates that the hydrocarbon species are unlikely to be on the Ru surface. Adsorption on the support is indicated by the observation of hydrocarbon bands on an alumina disk placed downstream of a catalyst disk and the report of similar bands when ethylene is adsorbed on η-alumina (32). Since α-olefins are the dominant C_{2+} hydrocarbons formed under the reaction conditions chosen for this study (6), it is reasonable to expect that the structures observed in the infrared spectra arise from the adsorption of these products at acid sites on the catalyst support. The carbonium ion thus formed would be stable in the absence of significant atomic hydrogen on the support surface. Since the surface of Ru is virtually saturated with CO under reaction conditions little hydrogen-spillover to the support would be expected. However, upon elimination of CO from the gas stream, the metal surface rapidly clears of adsorbed CO, and hydrogen can now adsorb freely. Spillover of hydrogen from the Ru to the alumina would then provide a source of atoms for removal of the adsorbed hydrocarbons.

CONCLUSIONS

The results of in situ infrared spectroscopy presented here demonstrate that the surface of a Ru/Al_2O_3 catalyst is covered primarily by linearly-adsorbed CO. The coverage by this species depends on the catalyst temperature and the CO partial pressure, and is found to obey a Langmuir isotherm, characterized by an equilibrium constant of $K_{CO} = 1.1 \times 10^{-9} \exp(25{,}000/RT)\ atm^{-1}$. Moderate concentrations of diadsorbed CO (e.g., $Ru(CO)_2$) and small concentrations of μ-bridge adsorbed CO (e.g., Ru-CO-Ru) were observed in addition to the linearly-adsorbed form. The first of these species appears to be associated with either individual Ru atoms or small Ru clusters, which interact strongly with the alumina support. In contrast to the linearly-adsorbed form of CO, diadsorbed CO does not react with H_2 at temperatures below 548K, and hence does not appear to participate in CO hydrogenation. The μ-bridged form of CO may occur in one of two possible forms. The first would be between a pair of Ru atoms, such that one atom bonds to the carbon end and the other Ru atom bonds to the oxygen end of the molecule. The second possibility is that the CO is attached through its carbon end to a Ru site and that the oxygen end interacts with a Lewis acid site on the support. Unfortunately, the amount of μ-bridge adsorbed CO detected is too small to make any definitive conclusions regarding its role in CO hydrogenation.

Bands associated with adsorbed hydrocarbon, formate and carbonate structures were also observed. The behavior of the hydrocarbon bands during and after reaction suggest that these structures are formed by the adsorption of olefinic hydrocarbons on the support. On the other hand, it appears that the formate and carbonate structures are formed on the surface of the alumina support via reactions of CO and H_2.

REFERENCES

1. Dalla Betta, R. A., and Shelef, M., J. Catal. 48, 111 (1977).

2. Ekerdt, J. G. and Bell, A. T., Preprints ACS Div. Petrol. Chem. 23, 475 (1978).

3. Ekerdt, J. G. and Bell, A. T., J. Catal. 58, 170 (1979).

4. King, D. L., Preprints ACS Div. Petrol. Chem. 23, 482 (1978).

5. King, D. L., J. Catal. 61, 77 (1980).

6. Kellner, C. S. and Bell, A. T., submitted to J. Catal.

7. Kuznetsov, V. L., Bell, A. T., and Yermakov, Yu. I., J. Catal. 65, 374 (1980).

8. Hicks, R. F., Kellner, C. S., Savatsky, B. J., Hecker, W. and Bell, A. T., submitted to J. Catal.

9. Tripathi, S. C., Srivastava, S. C., Mani, R. P., and Shrimal, A. K., Inorg. Chim. Acta. 15, 249 (1975).

10. Thomas, G. E., and Weinberg, W. H., J. Chem. Phys. 70, 1437 (1979).

11. Pfnür, H., Menzel, D., Hoffmann, F. M., Ortega, A., and Bradhsaw, A. M., Surface Sci. 93, 431 (1980).

12. Madey, T. E. and Menzel, D., Japan. J. Appl. Phys. Suppl. 2, Pt. 2, 229 (1974).

13. Feulner, P., Engelhardt, H. A., Menzel, D., Appl. Phys. 15, 355 (1978).

14. Williams, E. and Weinberg, W. H., Surface Sci. 82, 93 (1979).

15. Madey, T. E., Surface Sci. 79, 575 (1979).

16. Rabo, J. A., Risch, A. P. and Poutsma, M. L., J. Catal. 53, 295 (1978).

17. Low, G. G. and Bell, A. T., J. Catal. 57, 397 (1979).

18. Ku, R., Gjostein, N. A., and Bonzel, H. P., Surface Sci. 64, 465 (1977).

19. Fuggle, J. C., Umbach, E., Feulner, P., and Menzel, D., Surface Sci. 64, 69 (1977).

20. Reed, P. D., Comrie, C. M., and Lambert, R. M., Surface Sci. 59, 33 (1976).

21. Goodman, D. W., Madey, T. E., Ono, M., and Yates, Jr., J. T., J. Catal. 50, 279 (1977).

22. Pfnür, H., Feulner, P., Engelhardt, H. A., and Menzel, D., Chem. Phys. Lett. 59, 481 (1978).

23. Kettle, S. F. A. and Paul, I., Adv. Organmet. Chem. 10, 199 (1972).

24. Dalton, J., Paul, I., and Stone, F. G. A., J. Chem. Soc. A., 2744 (1969).

25. Yates, Jr., J. T., Duncan, T. M., Worley, S. D., and Vaughn, R. W., J. Chem. Phys. 70, 1219 (1979).

26. Dahl, L. F., Martell, C., Wampler, D. L., J. Am. Chem. Soc. 83, 1761 (1961).

27. Kellner, C. S. and Bell, A. T., submitted to J. Catal.

28. Colton, R., Commons, C. J., Haskins, B. F., J. C. S. Chem. Comm., 363 (1975).

29. Herrmann, W. A., Ziegler, M. L., Weidenhammer, K., and Biersack, H., Angew. Chem. Int. Ed. Engl. 18, 960 (1979).

30. Kristoff, J. S. and Shiver, D. F., Inorg. Chem. 13, 499 (1974).

31. Cant, N. and Bell, A. T., to be submitted to J. Catal.

32. Lucchesi, P. J., Carter, J. L., and Yates, D. J. C., J. Phys. Chem. 66, 1451 (1962).

CHAPTER IV

The Kinetics and Mechanism of Carbon Monoxide Hydrogenation Over Alumina-Supported Ruthenium

ABSTRACT

A study was conducted of hydrocarbon synthesis from CO and H_2 over an alumina-supported Ru catalyst. Rate data for the formation of methane and C_2 through C_{10} olefins and paraffins were fitted by power law rate expressions. The kinetics observed experimentally can be interpreted in terms of a comprehensive mechanism for CO hydrogenation, in which CH_x(x=0-3) species play a primary role. Expressions for the kinetics of methane synthesis, the kinetics and distribution of C_{2+} olefins and paraffins, and the probability of hydrocarbon chain growth derived from this mechanism are found to be in good agreement with the experimental results. The observed deviations from theory can be ascribed to secondary processes such as olefin hydrogenation and paraffin hydrogenolysis.

INTRODUCTION

During the past decade, extensive efforts have been made to understand the mechanism by which Group VIII metals catalyze the synthesis of hydrocarbons from CO and H_2 (1-7). One of the most important results of these investigations has been to draw attention to the importance of nonoxygenated surface intermediates. An increasing body of evidence now supports the hypothesis that hydrocarbon synthesis is initiated by the dissociation of CO and that the carbon atoms thus produced are hydrogenated to form adsorbed methylene and methyl groups. It has been proposed (5-7) that methyl groups act as precursors for the formation of methane as well as the growth of hydrocarbon chains, the latter process beginning with the insertion of a methylene group into the metal-carbon bond of a methyl group. Chain growth can continue by the further addition of methylene units to adsorbed alkyl species. Olefins and paraffins are finally produced from the alkyl moieties by either hydrogen elimination or addition.

A substantial part of the evidence supporting this view of hydrocarbon synthesis has been obtained from studies conducted with ruthenium catalysts. The emphasis on this metal can be explained by the fact that ruthenium produces, primarily, linear olefins and paraffins and relatively few oxygenated products. Moreover, unlike iron and cobalt, ruthenium is not converted to a carbide under reaction conditions. Studies by several authors (8-11) have shown that chemisorbed CO will dissociate on ruthenium at elevated temperatures to form adsorbed carbon atoms. Hydrogenation of this carbon occurs very readily to form methane as well as higher molecular weight paraffins. Ekerdt and Bell

(12) have shown that carbon deposition also takes place during the steady-state reaction of CO and H_2, and that hydrogenation of this carbonaceous deposit following the elimination of chemisorbed CO produces a spectrum of hydrocarbon products. These latter results demonstrate that chain growth can occur in the absence of adsorbed CO. Further evidence for the participation of atomic carbon in the growth of hydrocarbon chains has been obtained by Biloen et al. (11). In these studies nickel, cobalt, and ruthenium catalysts were precovered with ^{13}C atoms produced by the disproportionation of ^{13}CO. The adsorbed ^{13}CO was exchanged with ^{12}CO and the catalysts were then exposed to a mixture of ^{12}CO and H_2. Careful mass spectrometric analysis of the products showed a random distribution of ^{12}C and ^{13}C among the hydrocarbons, consistent with the initial inventories of the two isotopes. It was also found that the time needed to convert ^{13}C atoms and ^{12}CO molecules to methane were nearly identical. From these observations it was concluded that CO dissociation is very rapid and hence is unlikely to be a rate limiting step, that CH_x ($x = 0$-3) species constitute the most reactive C_1 surface species, and that methane and other hydrocarbons are formed from the same building blocks. These conclusions have also been supported by the analysis of methane synthesis kinetics reported by Ekerdt and Bell (12) and by the observation of a significant inverse H_2/D_2 isotope effect on methane synthesis recently reported by Kellner and Bell (13).

The proposition that hydrocarbon chain growth can occur on a ruthenium surface via a polymerization mechanism involving methylene groups as the monomer has recently been supported by the work of Brady and Petit (14). These authors demonstrated that a spectrum of hydrocarbons, resembling that obtained by CO hydrogenation, can be formed by reaction of CH_2N_2 and H_2 over ruthenium and other Groups VIII metals. The results were explained by suggesting that the decomposition of CH_2N_2 acts as a source of methylene groups, a part of which is converted to methyl groups by reaction with adsorbed hydrogen. It was proposed that the methyl groups then act as initiators for chain growth. The applicability of these results and their interpretation to hydrocarbon synthesis from CO and H_2 is supported by the work of Bell and coworkers (15,16). Their work has shown that methyl, methylene, and higher molecular weight alkyls present on a ruthenium surface can be detected through the reaction of these species with olefins, and that the consumption of surface methylene groups by this means inhibits the propagation of hydrocarbon chain growth.

In the present study an investigation has been carried out of the kinetics of hydrocarbon synthesis over an alumina-supported ruthenium catalyst. Emphasis was placed on establishing the influence of reaction conditions on the rates of product formation, the distribution of olefins and paraffins according to carbon number, and the ratio of olefin to paraffin obtained for each carbon number. These data were then used to evaluate theoretical expressions for the reaction kinetics, derived from a comprehensive mechanism for hydrocarbon synthesis.

EXPERIMENTAL

A 1% Ru/Al_2O_3 catalyst was prepared by adsorption of $Ru_6C(CO)_{17}$ from pentane solution on to Kaiser KA-201 γ-alumina. Details concerning synthesis of the complex and the impregnation procedure have been described previously (17). Once dried, the catalyst was reduced in flowing H_2. Reduction was begun by slowly raising the temperature from 298 to 673K and continued by maintaining it at 673K for 8 hr. The dispersion of the reduced catalyst was determined to be 1.0 by H_2 chemisorption.

A stainless steel microreactor heated in a fluidized bed was used for all of the work reported here. Reactants were supplied from a high-pressure cylinder containing a desired ratio of H_2 and CO. The reaction products were analyzed by gas chromatography using flame ionization detection. A balanced pair of 2.4 mm by 1 m stainless steel columns packed with Chromsorb 106 was used to separate C_1 through C_5 paraffins and olefins. A 0.25 mm by 35 m glass capillary column coated with OV-101 was used to separate C_5 through C_{10} paraffins and olefins. Complete product distributions were determined by normalizing the analyses for the C_5 products obtained from the packed and capillary columns.

Prior to each series of experiments, the catalyst (100 mg) was reduced in flowing H_2 for 10 to 12 hr at 673K and 10 atm. The temperature was then lowered to 498K and the feed mixture was introduced at a flow rate of 200 cm^3/min (NTP). Ten minutes after the reaction had begun, a gas sample was taken for analysis and the gas feed was switched over to pure H_2 for 1 hr. By alternating short reaction periods and longer reduction periods, a stable catalyst activity could be achieved after several cycles. Once this condition had been obtained the reaction conditions were adjusted to those desired for a particular experiment. Periodically, data were taken at 498K, 10 atm, and $H_2/CO = 3$ to determine whether changes in catalyst activity had occurred. In all cases, activities were reproduced to within a few percent. Maintaining the catalyst in H_2 for prolonged periods was also determined to have no effect on catalyst activity.

RESULTS

The rate of methane formation was measured at pressures between 1 and 10 atm, temperatures between 448 and 548K, and H_2/CO ratios of 1, 2, and 3. The accumulated data were fitted, by means of a nonlinear least squares regression, to the power law expresson given by eqn. 1,

$$N_{C_1} = 1.3 \times 10^9 \exp(-28{,}000/RT) P_{H_2}^{1.35} / P_{CO}^{0.99} \qquad (1)$$

In this equation, N_{C_1} is the rate of methane formation per second per surface Ru site, and P_{H_2} and P_{CO} are the partial pressures of H_2 and CO, respectively, expressed in atmospheres. Figure 1 illustrates the quality of agreement between rates calculated using eqn. 1 and those determined experimentally. The average deviation between experiment and correlation is less than $\pm$ 6%.

Seventy to eighty percent of the hydrocarbon products were analyzed to be C_2 through C_{10} paraffins and olefins. Examples of the ratio of the formation of hydrocarbons containing n carbon atoms to the rate of methane formation are shown in Figs. 2 and 3. Figure 2 shows that

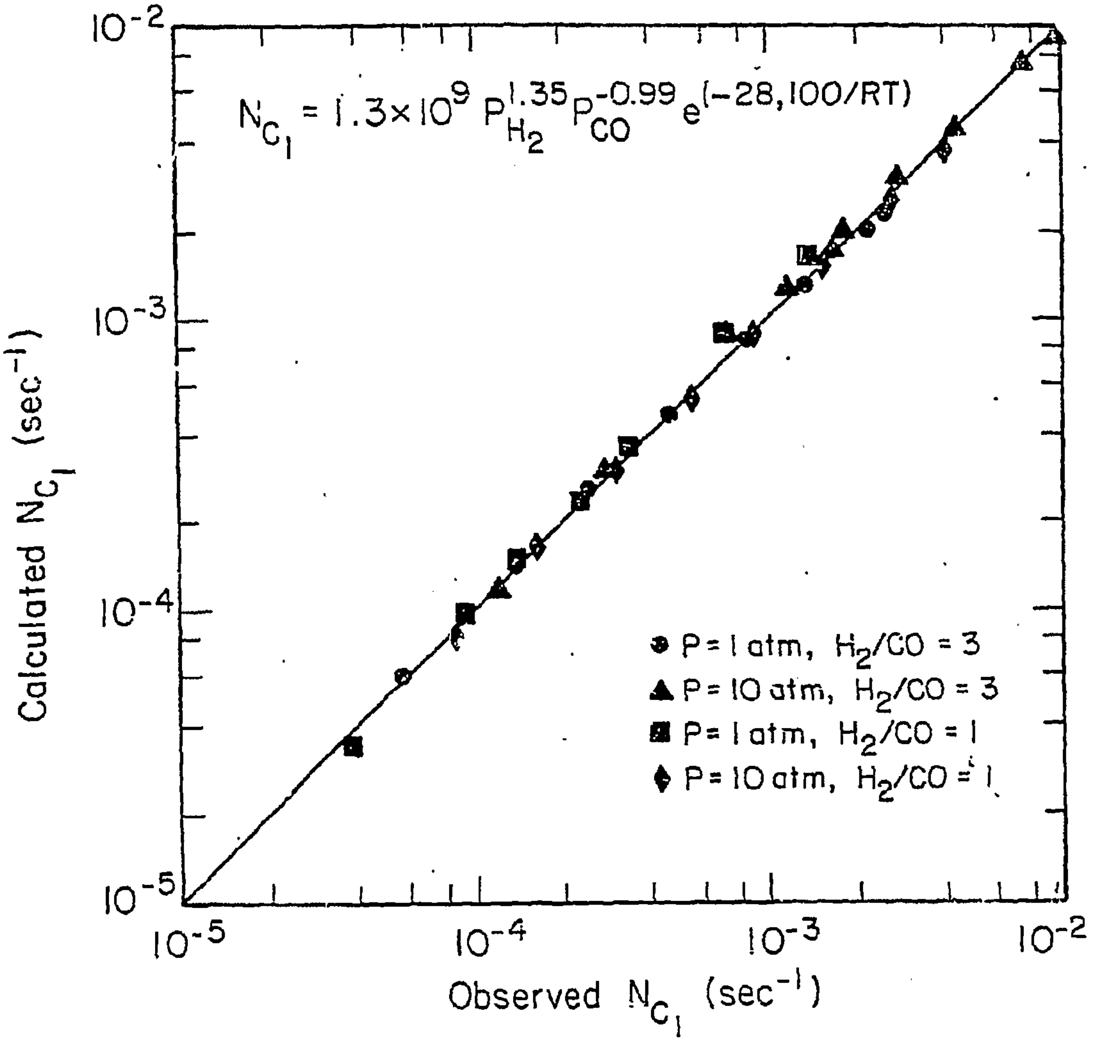

XBL 812-7918

Fig. 1. Cross-plot of predicted versus observed rates of methane synthesis.

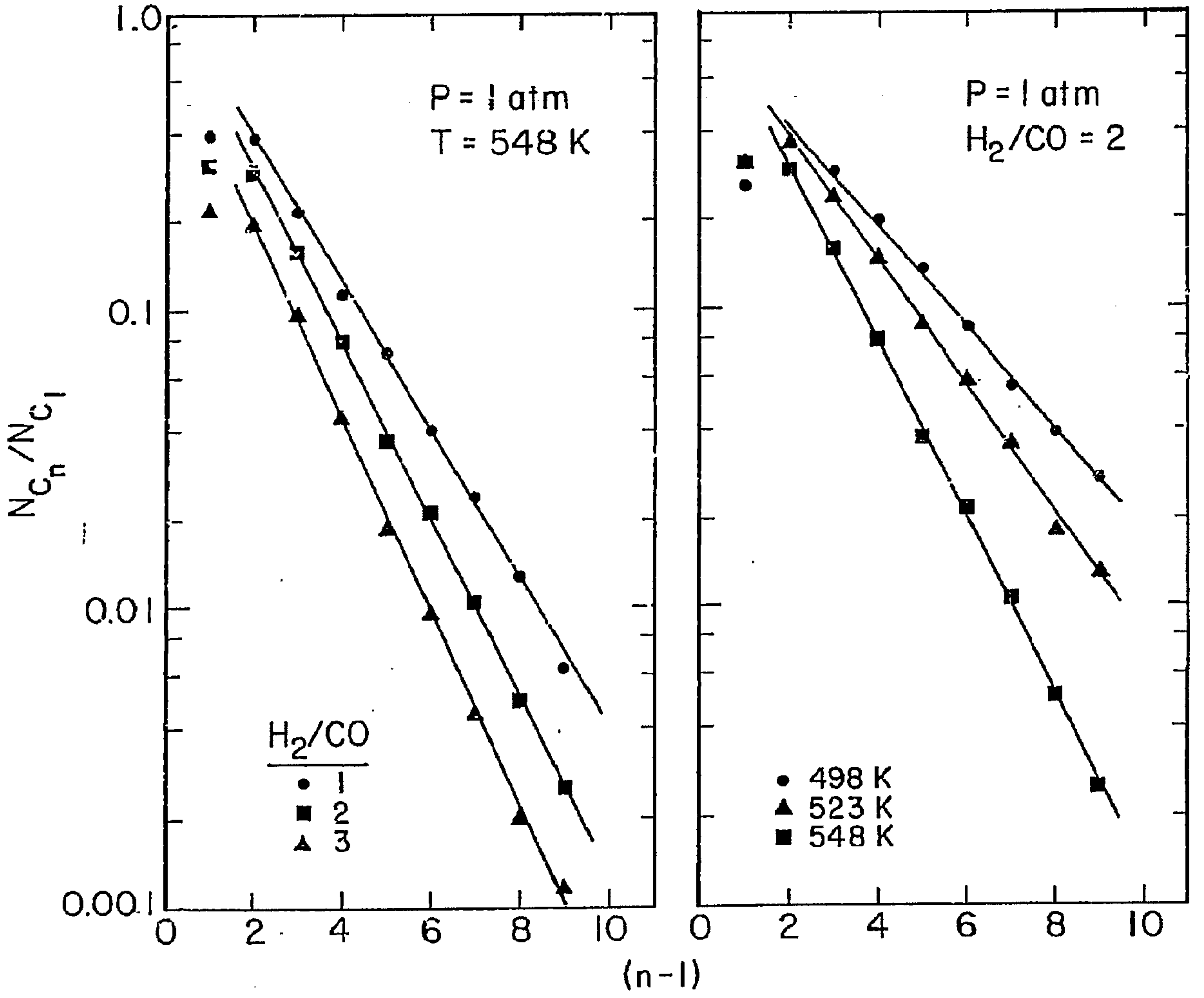

XBL 812-7927

Fig. 2. Distribution of C_1 through C_{10} hydrocarbons observed at 1 atm: a) effects of H_2/CO ratio; b) effects of temperature.

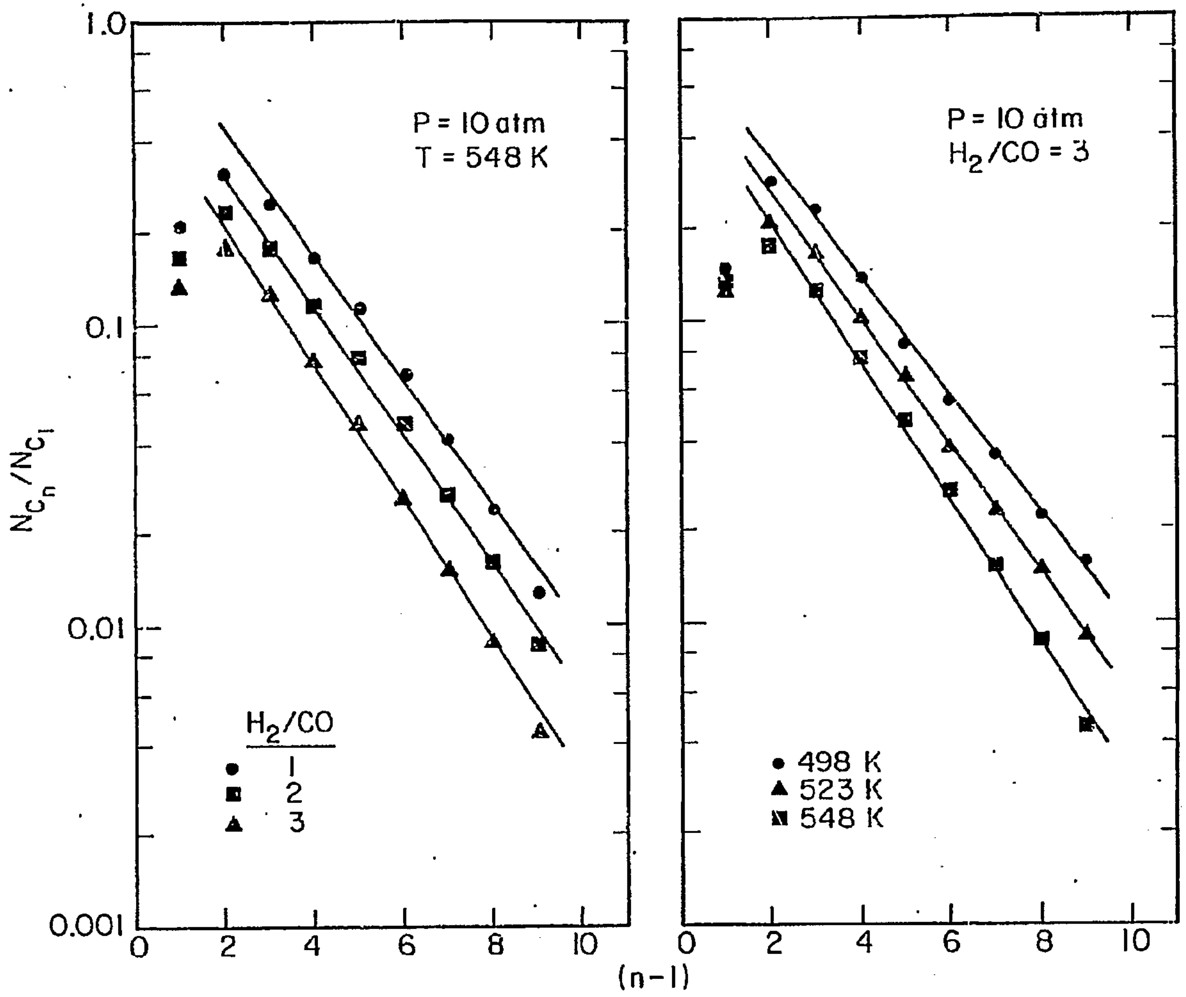

XBL 812-7928

Fig. 3. Distribution of C_1 through C_{10} hydrocarbons observed at 10 atm: a) effects of H_2/CO ratio; b) effects of temperature.

with the exception of the points for n=2 all of the data taken at 1 atm lie along straight lines on the coordinates of log (N_{C_n}/N_{C_1}) versus (n-1). The increasing slope of the lines as either the H_2/CO ratio or the temperature is decreased is indicative of an increase in the average molecular weight of the products. The data taken at 10 atm (Fig. 3) also lie along straight lines on the indicated coordinates, but in this case deviations are seen for n = 2 and 3. When either the H_2/CO ratio or the temperature is decreased, the slope of the lines in Fig. 3 increase slightly, and the lines appear to be translated upwards in a near parallel fashion.

The kinetics for the synthesis of C_2 through C_{10} olefins and paraffins can also be represented by power law rate expressions. Parameter values obtained by fitting the data to such expressions are presented in Tables I and II. Examination of Table I shows that a positive order dependence on H_2 and a negative order dependence on CO partial pressures is observed in all cases. For a given carbon number, the H_2 dependence for paraffin formation is higher than that for olefin formation, whereas the CO dependence is more nearly the same for both products. The data in Table II also indicate that the magnitudes of m and n for the formation of olefins decrease substantially with increasing carbon number. While there is some indication of a similar trend for the paraffins, the pattern is not as clearly evident as for the olefins.

The information presented in Table II shows that the activation energy for olefin synthesis is higher than that for paraffin synthesis, suggesting that the olefin to paraffin ratio in the products

Table I. Dependencies of the Rates for the Synthesis of C_1 through C_{10} hydrocarbons on the Partial Pressures of H_2 and CO^a.

	Olefin			Paraffin		
C_n	m	n	% Dev.[b]	m	n	%Dev.[b]
C_1	-	-	-	1.31	-0.96	7.7
C_2	0.82	-0.73	4.8	1.45	-0.85	7.7
C_3	0.80	-0.55	3.2	1.37	-0.49	4.9
C_4	0.74	-0.47	3.0	1.21	-0.46	3.3
C_5	0.53	-0.36	8.1	0.86	-0.24	2.3
C_6	0.47	-0.28	6.3	1.11	-0.32	13.5
C_7	0.35	-0.19	9.3	0.94	-0.24	5.9
C_8	0.31	-0.15	11.5	0.91	-0.27	7.9
C_9	0.20	-0.05	12.3	0.50	-0.18	19.4
C_{10}	0.17	-0.01	15.4	0.93	-0.35	11.4

[a] Reaction conditions: T = 498K; P = 1-10 atm; H_2/CO = 1-3

[b] Average deviation between predicted and observed rates.

Table II. Power Law Rate Expressions[a] for the Synthesis of C_1 through C_4 Hydrocarbons[b].

C_n	[A $atm^{(m-n)}s^{-1}$]	m	n	E_a(kcal/mole)	%Dev.[c]
C_1	1.3×10^9	1.35	-0.99	28	5.6
$C_2^{=}$	2.5×10^8	0.74	-0.68	28	5.7
C_2^{-}	1.6×10^6	1.34	-0.81	25	11.3
$C_3^{=}$	2.3×10^7	0.82	-0.58	25	4.2
C_3^{-}	1.4×10^3	1.39	-0.55	18	5.8
$C_4^{=}$	3.8×10^6	0.70	-0.44	24	9.6
C_4^{-}	8.7×10^3	1.14	-0.47	19	4.8

[a] $N_{C_n} = A \exp(-E_a/RT) P_{H_2}^{m} P_{CO}^{n}$

[b] Reaction conditions: T = 448-548K; P = 1-10 atm; H_2/CO = 1-3.

[c] Average deviation between predicted and observed rates

should increase with increasing temperature. The extent to which this trend is observed is illustrated in Fig. 4. Below about 498K, the plots of log $(N_{C_n^=}/N_{C_n^-})$ versus $1/T$ are linear for $n = 2,3$, and 4. From the slope of this portion of the plots, the difference in activation energies for the formation of olefins and paraffins is estimated to be about 6 kcal/mole. The sharp decline in log $(N_{C_n^=}/N_{C_n^-})$ which occurs at temperatures above 498K can be ascribed to hydrogenation of the olefins. This interpretation was confirmed by examining the effects of reactant space velocity on the olefin to paraffin ratio. At temperatures below 498K, this ratio is independent of space velocity, but as the temperature is increased above 498K, the ratio of olefins to paraffins decreases with decreasing space velocity.

Since it has been reported that olefins formed via primary reactions can be reincorporated to form higher molecular weight products (7,15), an investigation was made to establish the possible influence of such reactions on the observed product distributions. When ethylene was added to the synthesis gas at levels similar to those produced by the reaction, no evidence could be observed for olefin reincorporation. Raising the level of ethylene addition to 0.5 or 1.0% of the total feed (20 to 40 times that normally found in the reaction products) did produce an effect on the distribution of products, as can be seen in Fig. 5. The formation of C_3 and C_4 products is increased, but the formation of C_{6+} products is suppressed. The extent to which these changes occur increases with the level of ethylene addition. A similar trend was also observed for data taken at 1 atm and 498K.

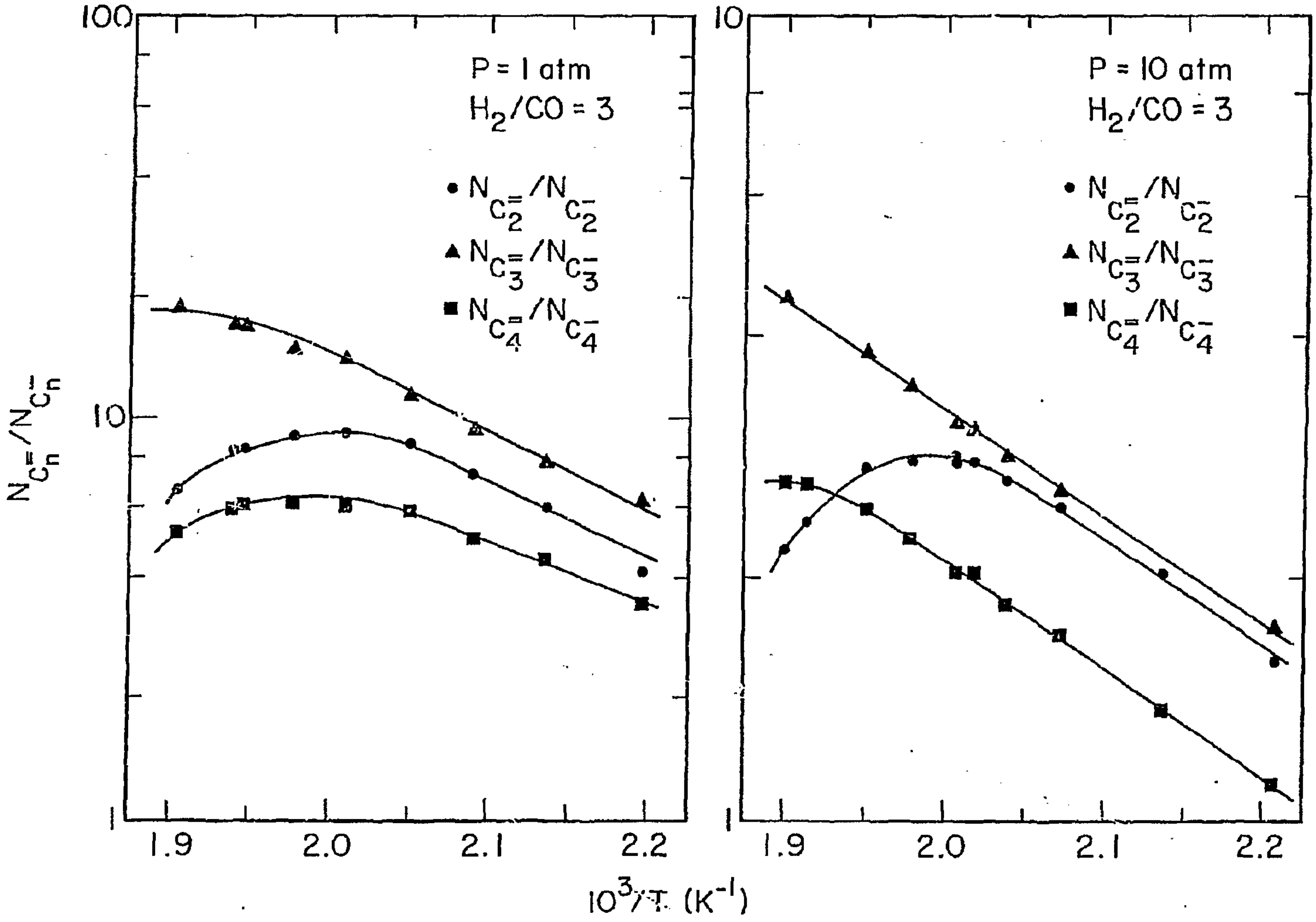

XBL 812-7929

Fig. 4. Effects of temperature on the olefin to paraffin ratio of C_2 through C_4 products: a) P = 1 atm; b) P = 10 atm.

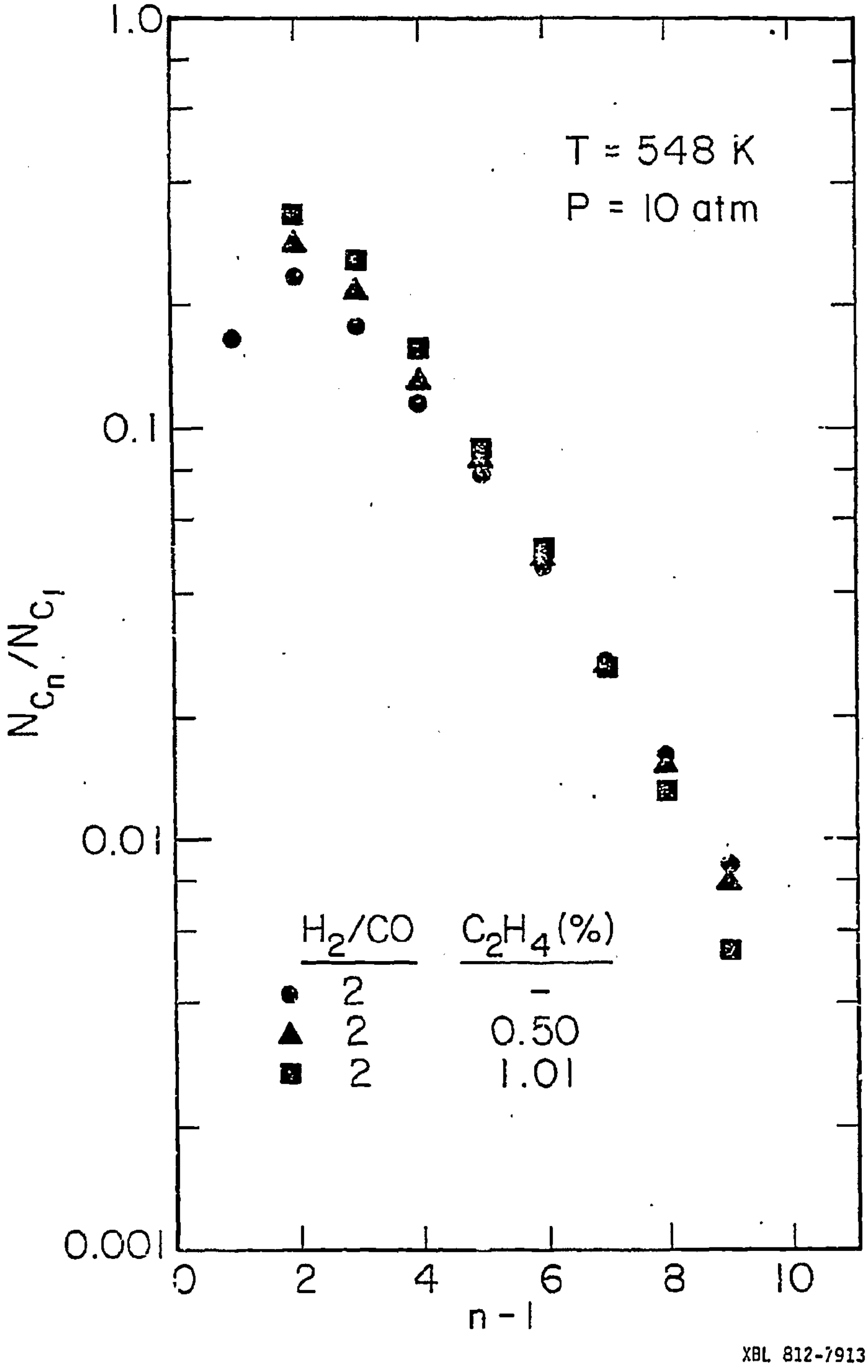

Fig. 5. Effects of ethylene addition on the distribution of C_1 through C_{10} hydrocarbons.

DISCUSSION

The kinetics of hydrocarbon synthesis presented here can be interpreted in terms of the mechanism shown in Fig. 6. Detailed discussions of the experimental evidence supporting this view of CO hydrogenation have recently been presented in a number of reviews (1-7). Consequently, the justification for including particular steps, and for assuming that certain of these are reversible, will be restricted to ruthenium.

It is proposed that CO is first adsorbed into a molecular state from which dissociative adsorption can then occur. Infrared studies reported by a number of authors (12,18-20) indicate that the surface of Ru is nearly saturated by molecularly adsorbed CO under reaction conditions. The reversibility of molecular adsorption is supported by recent isotopic substitution studies performed with ^{12}CO and ^{13}CO which indicate that equilibration of the surface with the gas phase is very rapid under reaction conditions (21). Low and Bell (10) have shown that CO disproportionation will occur to a significant degree over Ru/Al_2O_3 for temperatures in excess of 423K. These results suggest that CO dissociation is an activated process. More recently, TPD experiments performed by McCarty and Wise (22) have demonstrated that the recombination of carbon and oxygen atoms and the desorption of CO are very rapid since extensive scrambling of preadsorbed $^{13}C^{16}O$ and $^{12}C^{18}O$ was observed at temperatures above 473K, where hydrocarbon synthesis normally occurs.

The adsorption of H_2 is assumed to occur dissociatively, and to be reversible. This view is supported by H_2/D_2 scrambling studies

1. $CO + S \rightleftharpoons CO_s$
2. $CO_s + S \rightleftharpoons C_s + O_s$
3. $H_2 + 2S \rightleftharpoons 2H_s$
4. $O_s + H_2 \rightarrow H_2O + S$
5. $C_s + H_s \rightleftharpoons CH_s + S$
6. $CH_s + H_s \rightleftharpoons CH_{2_s} + S$
7. $CH_{2_s} + H_s \rightleftharpoons CH_{3_s} + S$
8. $CH_{3_s} + H_s \rightarrow CH_4 + 2S$
9. $CH_{3_s} + CH_{2_s} \rightarrow C_2H_{5_s} + S$
10. $C_2H_{5_s} + S \rightarrow C_2H_4 + H_s + S$
11. $C_2H_{5_s} + H_s \rightarrow C_2H_6 + 2S$
12. $C_2H_{5_s} + CH_{2_s} \rightarrow C_3H_7 + S$

etc.

Fig. 6. Proposed mechanism of hydrocarbon synthesis from CO and H_2.

performed in the presence of CO over a Ru/SiO_2 catalyst (21). The results of these experiments show that above 423K, the extent of scrambling is very close to that predicted at equilibrium, indicating that the rates of $H_2(D_2)$ adsorption, reaction, and desorption are faster than the rate of hydrocarbon synthesis.

It is well recognized that during CO hydrogenation over Ru, water is the primary product via which oxygen is removed from the catalyst surface (12). The mechanism of forming water in the presence of substantial amounts of adsorbed CO is not known and may occur via either a sequence of Langmuir-Hinshelwood steps or a concerted Rideal-Eley step. For the purposes of the present discussion it has been assumed that the latter process represents the dominant reaction path.

The stepwise hydrogenation of single carbon atoms is taken as the starting point for hydrocarbon synthesis. Studies by a number of investigators (9-11) have shown that atomic carbon produced by either CO disproportionation or CO hydrogenation is extremely reactive and will form methane and higher molecular weight hydrocarbons upon hydrogenation. Furthermore, the work of Biloen et al. (11) has demonstrated that the incorporation of carbon into hydrocarbons occurs with equivalent ease from molecularly adsorbed CO and atomically adsorbed C, indicating that the dissociation of adsorbed CO is not a rate limiting step in the formation of hydrocarbons. This conclusion is supported further by the recent studies of Kellner and Bell (13) in which evidence was reported for a strong inverse H_2/D_2 isotope effect on the synthesis of methane over two Ru/Al_2O_3 catalysts and a similar albeit weaker effect for synthesis over a Ru/SiO_2 catalyst. The authors noted that